APL MATERIALS 6, 080701 (2018)

Research Update: Recent progress on 2D materials beyond graphene: From ripples, defects, intercalation, and valley dynamics to straintronics and power dissipation

Zhong Lin,[1,2,a] Yu Lei,[2,3,a] Shruti Subramanian,[2,3,a] Natalie Briggs,[2,3,a] Yuanxi Wang,[1,2,4] Chun-Li Lo,[5] Eilam Yalon,[6] David Lloyd,[7] Sanfeng Wu,[8] Kristie Koski,[9] Richard Clark,[10] Saptarshi Das,[11] Robert M. Wallace,[12] Thomas Kuech,[13] Joseph Scott Bunch,[14] Xiaoqin Li,[15] Zhihong Chen,[5] Eric Pop,[6] Vincent H. Crespi,[1,2,3,4,16] Joshua A. Robinson,[2,3,4,16] and Mauricio Terrones[1,2,3,16,17,b]

[1]*Department of Physics, The Pennsylvania State University, University Park, Pennsylvania 16802, USA*
[2]*Center for 2-Dimensional and Layered Materials, The Pennsylvania State University, University Park, Pennsylvania 16802, USA*
[3]*Department of Materials Sciences and Engineering, The Pennsylvania State University, University Park, Pennsylvania 16802, USA*
[4]*2-Dimensional Crystal Consortium, The Pennsylvania State University, University Park, Pennsylvania 16802, USA*
[5]*School of Electrical and Computer Engineering and Birck Nanotechnology Center, Purdue University, West Lafayette, Indiana 47907, USA*
[6]*Department of Electrical Engineering, Stanford University, Stanford, California 94305, USA*
[7]*Department of Mechanical Engineering, Boston University, Boston, Massachusetts 02215, USA*
[8]*Department of Physics, Massachusetts Institute of Technology, 77 Massachusetts Avenue, 13-2037, Cambridge, Massachusetts 02139, USA*
[9]*Department of Chemistry, University of California Davis, Davis, California 95616, USA*
[10]*Carbon Science Center of Excellence at Morgan Advanced Materials, State College, Pennsylvania 16802, USA*
[11]*Engineering Science and Mechanics, Pennsylvania State University, University Park, Pennsylvania 16802, USA*
[12]*Department of Materials Science and Engineering, The University of Texas at Dallas, Richardson, Texas 75080, USA*
[13]*Department of Chemical Engineering, University of Wisconsin Madison, 1415 Engineering Dr., Madison, Wisconsin 53706, USA*
[14]*Division of Materials Science and Engineering, Boston University, Brookline, Massachusetts 02446, USA*
[15]*Physics Department and Center for Complex Quantum System, University of Texas at Austin, Austin, Texas 78712, USA*
[16]*Center for Atomically Thin Multifunctional Coatings (ATOMIC), The Pennsylvania State University, University Park, Pennsylvania 16802, USA*
[17]*Department of Chemistry, The Pennsylvania State University, University Park, Pennsylvania 16802, USA*

(Received 2 June 2018; accepted 23 July 2018; published online 10 August 2018)

The field of two-dimensional (2D) materials has witnessed several significant advancements in a short period of time. There have been extensive research efforts dedicated to this field and an expanding community of researchers built around the same. The focus of this review article is on the most recent milestones in several aspects of 2D materials with emphasis on transition metal dichalcogenides, such as improved synthesis and property engineering, approaching this from both experimental and theoretical viewpoints. There is also an attempt at highlighting some emerging material properties that are of interest and use of these 2D materials in

[a]Z. Lin, Y. Lei, S. Subramanian, and N. Briggs contributed equally to this work.
[b]Author to whom correspondence should be addressed: mut11@psu.edu

 © Author(s) 2018

several electronic applications. © *2018 Author(s). All article content, except where otherwise noted, is licensed under a Creative Commons Attribution (CC BY) license (http://creativecommons.org/licenses/by/4.0/).* https://doi.org/10.1063/1.5042598

I. INTRODUCTION

More than ten years after the isolation of graphene,[1] the field of two-dimensional (2D) materials continues to evolve rapidly. Since the experimental demonstration of graphene in 2004, the number of publications per year related to 2D materials continues to increase. According to Web of Science, in 2010, over 3000 papers were published on 2D materials. In 2013, this number increased to over 9000 and in 2017, further increased to greater than 17 000. Such substantial interest in this field can be attributed to the rich platforms that 2D materials provide for studying a variety of different topics,[2] from fundamental physics[3,4] to (opto)electronics,[5] energy,[6,7] and biology.[8]

For the purposes of this article, "2D materials" refer to materials which are thermodynamically stable in layers that are just a few atoms thick [e.g., graphene is one atom thick and monolayer (1L) MoS_2 is three atoms thick], exhibiting properties that are different from their bulk, layered counterparts (e.g., graphite). Following the demonstration of a number of fascinating 2D materials, such as transition metal dichalcogenides (TMDs), synthesis[9] and material defects[10,11] have emerged as a primary focus of 2D materials research today, with challenges remaining in the realization of large-area systems that can compete with exfoliated (highly crystalline) layers, as well as a detailed understanding of defect types and their effects in 2D layers. Additionally, fundamental physical phenomena continue to be studied and the development of effective device architectures is now pushing 2D materials toward novel technological applications. This article highlights a number of studies in the field of 2D materials that include synthesis (see Sec. II), property engineering via defects and intercalation (see Sec. III), valleytronic and topological properties (see Sec. IV), and electronic applications (see Sec. V). It also provides insight into the current directions of 2D materials research and discusses areas requiring further investigation (see Sec. VI). The main materials of focus in this article are TMDs, and the highlighted topics reflect the content of the annual Graphene and Beyond workshop at the Pennsylvania State University, in which a diverse group of experts discussed recent advancements in this exciting field.

II. SYNTHESIS

The synthesis of 2D materials includes several key routes: mechanical exfoliation, chemical exfoliation, and direct synthesis. To date, mechanical exfoliation tends to result in higher quality single crystal materials that can exhibit near-ideal electronic behavior.[12] Exfoliation and transfer techniques have evolved rapidly and have led to the development of advanced layered heterostructures of different 2D systems [also known as van der Waals (vdW) solids], which in turn lead to the understanding of new physical phenomena. However, exfoliation techniques fall short in terms of scalability. In comparison, direct synthesis of 2D materials offers advantages in scalability. Rather than thinning a bulk material down to a single atomic or molecular sheet, direct synthesis aims at growing 2D materials via bottom-up synthetic techniques over large areas. Synthetic strategies include a variety of vapor deposition techniques (chemical, physical, and metalorganic).[13–15] Challenges that 2D material synthesis faces are quite similar to those faced in bulk crystal growth, such as producing large single crystal domains with low defect density and the ability to tailor material properties. Despite these challenges, the field of 2D materials continues to advance, with improvements in material quality and processing, together with a growing palette of emerging 2D materials, and the development of novel synthetic strategies.[16]

The use of chemical vapor deposition (CVD) has been evolving rapidly, and the challenges lie in the difficulties for nucleation of a monolayer thick single crystal.[17] Many active areas of research for nucleation control currently exist, some of which include substrate composition modification, chemical pretreatment, functionalization, and growth temperature modification.[18–20] Obtaining uniform, high-density, and highly oriented initial growth islands is difficult to achieve, and will remain

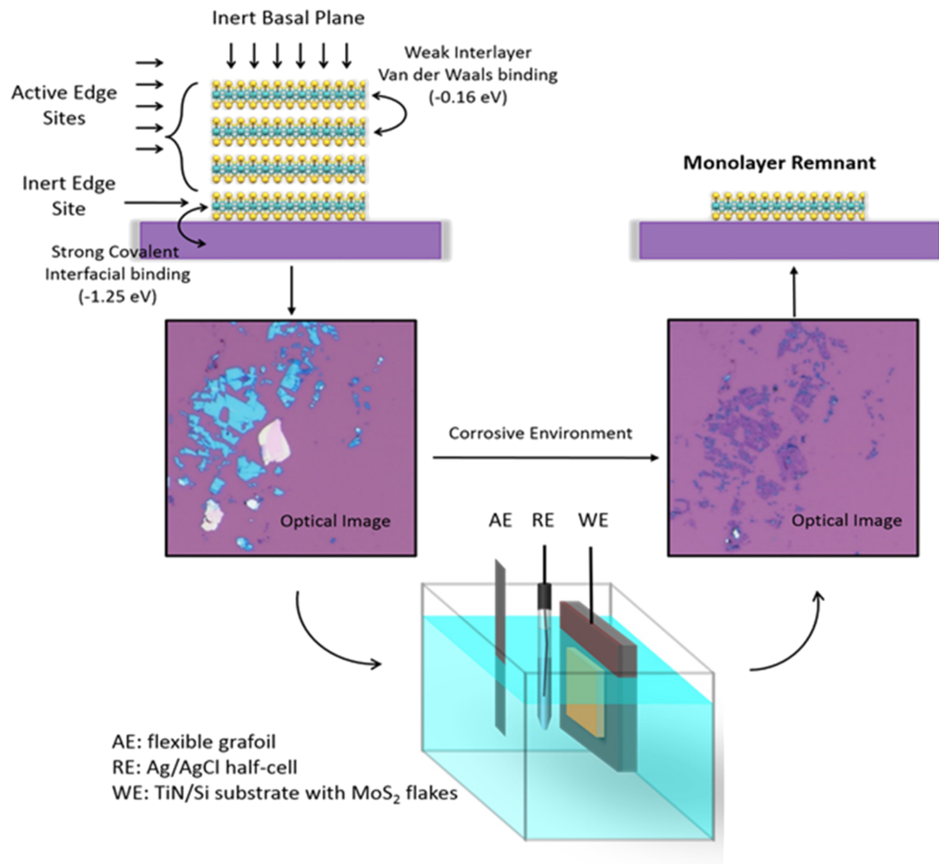

FIG. 1. Schematic of the electro-ablation (EA) process for the synthesis of monolayer MoS_2, WS_2, and $MoSe_2$ from exfoliated bulk materials. The strong covalent interaction of the monolayer with the substrate in comparison to weak vdW interaction between the layers results in the enhanced stability of the monolayer in the oxidizing corrosive environment which otherwise etches the bulk material. Reprinted with permission from Das *et al.*, Sci. Rep. **6**, 28195 (2016). Copyright 2016 Springer Nature.

an ongoing challenge. Once achieved, the formation of vertical and lateral heterostructures uniformly over large areas will allow a more widespread extension of these materials into device technologies.

In addition to vapor phase techniques, solution chemical routes to generate 2D materials are also available. In this context, solution-based synthesis offers many advantages. In particular, wet chemical reactions can easily be scaled-up to produce greater quantities of 2D materials.[21–24] This provides a wider range of material control along with reduced growth costs. Wet chemical routes however suffer from one major drawback; they tend to aggregate into multi-layers rather than single monolayers. One new method for achieving monolayers, however, falls in the realm of electrochemical exfoliation. Recently, Das *et al.* reported that multi-layer TMD flakes can be converted into monolayers through exposure to highly oxidizing and corrosive environments (Fig. 1). These studies showed that monolayers were achievable in such environments at room temperature within just a few seconds.[25]

III. PROPERTY ENGINEERING OF 2D MATERIALS

Despite great efforts to improve the crystalline quality of synthesized 2D materials, defects remain present. Understanding and controlling synthetic defects constitutes a key step in engineering the properties of 2D materials. This section highlights work to tailor the properties of 2D materials along the line of defect engineering, shedding light on the effects of fluctuating growth conditions and ripples on defect formation, as well as investigations of heteroatoms within and between 2D layers. It also elucidates the engineering properties of 2D materials via intercalation.

A. Property engineering via defects

1. Kinetic control of defects in 2D TMD materials

2D sheets can host one-dimensional (1D) anisotropies in both shape and composition, and this can affect materials properties and reflect characteristics of materials growth and processing. For example, the catalytic, electronic, transport, and optical properties[26–36] of 2D systems can be profoundly affected by dopants or alloying, which need not be isotropic (invariant with respect to the direction) or homogeneous (invariant with respect to the location). The spatial distribution of transition metal atoms in alloys may assume a 1D "striped" character, apparently driven by kinetic effects at the edge of the growing flake.[37] Interestingly, this form of order appears to originate from fluctuations under growth conditions, in that the preferred metal at the growth edge of $W_xMo_{1-x}S_2$ near $x = 0.5$, depends on the sulfur chemical potential, and is insensitive to the composition deeper within the flake. Local fluctuations in sulfur availability along the 1D growth edge translate into stripe-like distributions of W and Mo atoms within the 2D layer. The large mass difference between Mo and W could then cause significant anisotropies in vibrational and thermal properties by, e.g., introducing phonon anomalies at wave vectors commensurate to the stripes, and wider stripes could provide a means to modulate electronic properties across multiple length scales. More generally, the fact that the equilibrium structural energetics in certain 2D alloy systems such as $W_xMo_{1-x}S_2$ can be made agnostic to metal type and arrangement opens up kinetic mechanisms as a means to control alloy order during growth.

Folds or "ripples," like what may form in a poorly installed carpet, provide another example of a 1D anisotropy hosted by a 2D sheet.[38] Such ripples induce localized strain that modulates the bandgap of the host material[39] and also define local curvatures that couples favorably to lattice defects—specifically chalcogen vacancies, which have lower formation energies in concave regions of the TMD sheet[40] (in contrast to the preferential fluorination of curved sp^2 carbon, which occurs in regions with higher convexity[41]). Such a local environment is present in the lower chalcogen layer along the ridgeline of the ripple (blue circles in Fig. 2) and also in the upper layer of chalcogenide

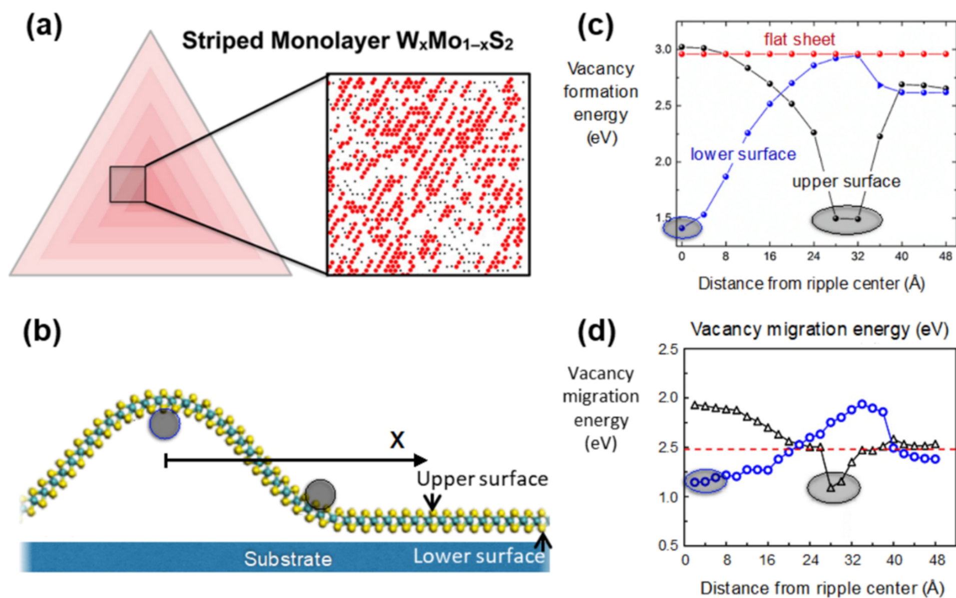

FIG. 2. (a) Schematic figure of a triangular flake of the $W_xMo_{1-x}S_2$ alloy with Mo content increasing from the edge to center. Reprinted with permission from Azizi *et al.*, Nano Lett. **16**(11), 6982–6987 (2016). Copyright 2016 American Chemical Society. (b) A fold (or "ripple") hosts two types of locally concave regions with lower vacancy formation energies: the lower chalcogen surface along the ridgeline at the top of the ripple (blue circle) and the top chalcogen surface at the base of the ripple (black circle). The two regions can also be identified from (c) the sulfur vacancy formation energy as a function of defect location x, blue for the lower chalcogen surface and black for the upper one, and (d) the vacancy diffusion barrier across the same spatial range. The energy landscapes for a flat sheet are shown with red lines. [(b)–(d)] Reprinted with permission from Ostadhossein *et al.*, J. Phys. Chem. Lett. **8**(3), 631–640 (2017). Copyright 2017 American Chemical Society.

along the upward curving region at the base of the ripple (black circles). Local concavity around the vacancy apparently ameliorates the bond angle and bond distance stresses associated with the absence of the chalcogen. Calculations within a classical empirical potential, ReaxFF, indicate that this energetic preference is significant, on the order of ∼1 eV per vacancy for moderate sheet curvatures.[40] Thus, ripples will tend to pin in locations with high vacancy density and conditions that facilitate vacancy migration may enable curvature inhomogeneities, such as ripples, to trap and potentially transport vacancies in certain regions of the sheet. Going beyond experimentally well-characterized isolated ripples in 2D systems, control over junctions joining more than two ripples[42,43] (a common consequence of the thermal expansion coefficient mismatch between the substrate and the 2D overlayer) and over the placement of ripples (or folds in general) remains a challenge for the future.[44]

These two defect types, metal substitutions and chalcogen vacancies, can also interact with each other. For example, at low densities of Mo within WS_2, the substitutional Mo can exhibit a pronounced tendency to co-locate with sulfur vacancies.[45] Computationally, the energetic affinity of these two species is weak for the charge-neutral case, but rises substantially for n-type systems, due to the partial occupation of a mid-gap state that is degenerate in the pure WS_2 system but becomes symmetry-split in the presence of Mo in the local environment. The presence of Mo also lowers the Fermi level required to stabilize a negatively charged mid-gap state. The cross-coupling of substitutional dopants, sheet curvature, and chalcogen vacancies thus provide multiple possible routes toward modulating the prevalence and location of various local defects in 2D TMDs.[40,46]

2. Characterizing defects in 2D TMD materials

In order to investigate defects in these materials, a combination of techniques with varying detection limits is used. In many samples, the impurity levels are below the detection limit of typical surface analytical methods (∼0.1-1 at. % corresponding to 10^{12}-10^{13} atoms/cm^2), so careful studies must rely on mass spectrometry methods, such as inductively coupled plasma mass spectrometry (ICPMS) where detection ranges down to ∼10^6 atoms/cm^2. By contrast, surface/bulk defect, interfacial chemistry, and structural studies can be amply studied by methods such as electron microscopy, photoelectron spectroscopy, electron diffraction, and scanning tunneling microscopy/spectroscopy. For device applications, where carrier scattering from such impurities and defects degrades mobility, an assessment of their concentration is necessary to minimize performance degradation.[47,48] Impurity analysis of W-based TMDs provides an example of utilizing ICPMS to gauge the concentration of impurities in TMD materials.[49,50] Some authors have shown the ICPMS analysis of WS_2, WSe_2, and WTe_2 commercially grown by chemical vapor transport, with the concentrations normalized to a Si-host matrix.[48] This is done to gauge the concentration in view of the Si-based integrated circuit industry standards, which require certain impurities (e.g., those that lead to trap states in Si) to be limited to 5×10^{10} atoms/cm^2 or less.[51] It is clear that the impurity levels from recent, commercially synthesized TMDs can be kept below the specification levels of the Si-based integrated circuit (IC) industry.[49] This is in contrast to earlier analysis of geological and synthesized TMDs, such as MoS_2, where some impurities can exceed 5×10^{10}/cm^2.[52] Thus, material growers have established procedures and protocols to enable high quality TMD materials from an impurity perspective and thus enable better device electronic performance. Generally, although the synthesis of TMDs has improved from an impurity perspective, control of defects (e.g., chalcogen vacancies) and grain size in thin films still presents challenges that must be overcome for the mainstream Si IC industry. Further work is needed to establish protocols for impurity analysis in synthesized thin TMD films, such as using laser ablation ICPMS. Defect passivation is also an activity requiring further study to enable thin TMD films with high electronic performance.

B. Property engineering via intercalation

While defects arising from variations in growth conditions or material geometry are often unintentional, purposefully inducing defects in 2D materials can provide unique opportunities in the realm of materials engineering and design. A core feature of a layered material is the vdW spacing, which can host guest atoms, ions, molecules, and other types of intercalants between the 2D planes. Intercalation of layered materials has long enabled applications such as energy storage, solid lubrication, and electrochromics.[51,53,54] Intercalation can also alter fundamental phase behavior modifying phase

transitions, e.g., varying superconducting transition temperatures[51,53,55] and modulating charge density wave transitions.[53] Generally, intercalation is achieved by electrochemically moving ions in and out of the host or by refluxing the layered materials in an organic liquid so as to push molecules in the vdW spacings.[51]

Zero-valent intercalation is a relatively new chemistry method able to alter 2D layered materials. Since the intercalant has no ionic charge, very large concentrations of zero-valent metals, such as Ag, Bi, Cu, Co, Sn, In, etc., can be reversibly intercalated into the gap.[56–59] For example, up to 60 at. % copper or 60 at. % silver has been intercalated into Bi_2Se_3.[58,59] Zero-valent intercalation is general and not constrained by crystallinity, phase purity, or morphology. It works in powders, single-crystals, or nanocrystals and for chalcogens, oxides, and graphite-based compounds. In order to intercalate zero-valent metals, a zero-valent metal atom is generated in solutions such as a disproportionation redox reaction or carbonyl decomposition [Fig. 3(a)]. Deintercalation can be performed using the reverse comproportionation redox reaction as shown with Cu and Sn below:[56]

$$\text{Intercalation: } 2Cu^{+}(aq.) \rightleftharpoons Cu^{0} + Cu^{2+}(aq.) \quad \text{Deintercalation: } Cu^{0} + Cu^{2+}(aq.) \rightleftharpoons 2Cu^{+}(aq.)$$

$$\text{Intercalation: } 2Sn^{2+}(aq.) \rightleftharpoons Sn^{0} + Sn^{4+}(aq.) \quad \text{Deintercalation: } Sn^{0} + Sn^{4+}(aq.) \rightleftharpoons 2Sn^{2+}(aq.)$$

Since the intercalant is zero-valent, multiple atomic species (such as CuFe and CoSn) can be intercalated to form an alloy-like metal layer within the host.[60] Figure 3(b) shows an example of a superlattice electron diffraction pattern formed from Cu intercalation in Bi_2Se_3 followed by Fe intercalation. In electrochemical intercalation, this would be difficult because ionic species repel each other and have different redox potentials that limit their co-intercalation ability. Intercalated metals form an atomically thin monolayer or bilayer of a quantum confined metal within a host. Intercalant guests can self-organize resulting in superlattice structures [Fig. 3(b)], temperature and concentration polytypic phase transitions,[61,62] and incommensurate Pokrovsky-Talapov transitions.[61] Zero-valent intercalation alters opto-electronic and catalytic properties. Intercalation of copper into Bi_2Se_3 makes the materials more optically transparent [Fig. 3(c)] which is reversible with deintercalation [Fig. 3(d)].[56] Intercalation of zero-valent Co and Sn into MoO_3 causes a reversible chemochromic color change from transparent white to dark blue. Addition of hydrogen peroxide deintercalates the metal reverting the color. Intercalated Co- and Sn-MoO_3 can also be altered from dark blue to white, coinciding with a disorder-order phase transition of the intercalated Co and Sn metal.[56,62] Zero-valent copper intercalated Birnessite shows an almost four-fold enhancement as a water oxidation catalyst.[63]

As a route to chemically alter 2D materials *in situ* or *in operando*, zero-valent intercalation can offer dynamic adaptation of material chemical and physical properties. It can provide access to an enormous new range of material structures with properties unattainable with a single species. The

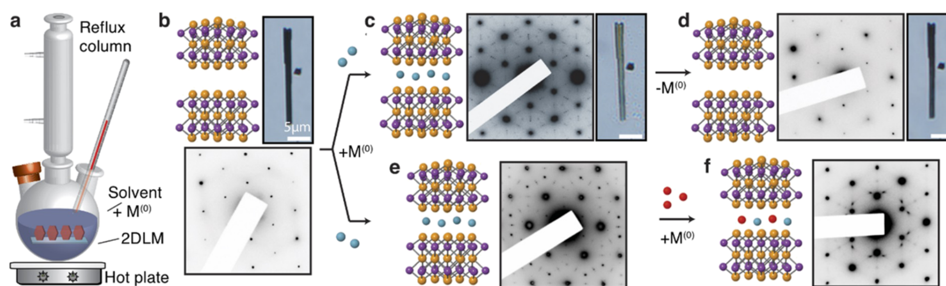

FIG. 3. (a) Zero-valent intercalation is performed typically at low temperature (e.g., 50 °C in acetone) just below reflux. (b) An example of Bi_2Se_3 which shows (c) superlattice peaks with Cu intercalation and is more transparent. (d) Superlattice peaks disappear with deintercalation along with a return in opacity. (e) Cu-intercalated Bi_2Se_3 can also be co-intercalated as (f) CuFe-Bi_2Se_3 forming unique superlattice diffraction patterns. Reprinted with permission from Wang *et al.*, Chem. Mater. **29**(4), 1650–1655 (2017). Copyright 2017 American Chemical Society. Reprinted with permission from Chen *et al.*, J. Am. Chem. Soc. **137**(16), 5431–5437 (2015). Copyright 2015 American Chemical Society. Reprinted with permission from M. Wang and K. J. Koski, J. Phys.: Condens. Matter **28**(49), 494002 (2016). Copyright 2016 IOP Publishing.

next goal of this chemistry is the zero-valent intercalation of semiconductors, heavier metals, and superconductors.

IV. EMERGING PHYSICAL PROPERTIES OF 2D TMD MATERIALS

Despite significant advancements in material synthesis and application of 2D materials in more traditional device architectures, much investigation remains in the realm of physical properties of 2D materials. This section reviews recent advancements in the valleytronic and topological properties of TMDs, as a subset of 2D materials. Such work aids understanding fundamental phenomena within 2D TMD materials and opens the door to their implementation in advanced information technologies.

A. Valley dynamics in monolayer TMDs

2D materials hold potential for a range of applications in information technology. For example, monolayer TMDs show promise as potential materials to encode and process information. This potential stems from the fact that monolayer TMDs have hexagonal lattice structures and their extrema (i.e., valleys) of energy-momentum dispersion curves appear at two degenerate K and K' points at the edges of the Brillouin zone [Fig. 4(a)]. Excitons are formed at the K and K' points with inherent spin and valley degree of freedoms (DoF). As with any binary quantum DoF, the valley pseudospin can be modeled as a two-level system and represented by a Bloch vector, the quantum dynamics of which can be conceptualized by a vector evolving on the Bloch sphere shown in Fig. 4(b).

Encoding and processing information based on the valley pseudospin requires creating electrons or excitons exclusively in one valley, a task readily accomplished by leveraging the valley-contrasting optical selection rules shown in Fig. 4(a). Using $\sigma_+(\sigma_-)$ polarized optical excitation, excitons are created in the $K(K')$ valley, which initializes the valley pseudospin Bloch vector along the North (South) pole.[64–67] The valley DoF can be further manipulated with a magnetic field or an ultrafast pulse.[68–74] If instead linearly polarized optical excitation is used, the exciton is initialized into a quantum mechanical coherent superposition of equal occupancy in both K and K' valleys.[75,76] Such a coherent state is represented as a vector in the equatorial plane of the Bloch sphere. The dynamics of this valley DoF are characterized by longitudinal (T_1) and transverse relaxation time (T_2) corresponding to valley depolarization and valley decoherence, respectively.

One prominent quasiparticle resonance in TMDs is a trion or charged exciton.[77] A negatively charged trion consists of two electrons and one hole. A trion appears at a lower energy than an exciton by an energy shift known as the trion binding energy. The trion binding energy is in the range of 20-40 meV in monolayer TMDs (comparable to thermal excitation energy at room temperature), a value approximately one order of magnitude larger than that in GaAs quantum wells.[78] Trions, as charged composite quasiparticles, can be detected in transport measurements as well. Thus, they serve

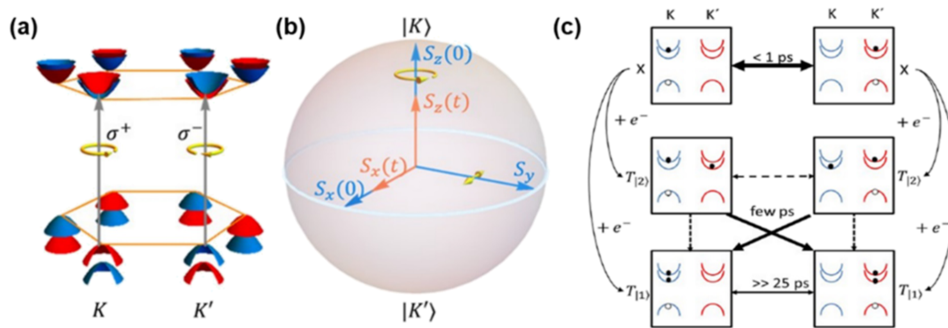

FIG. 4. (a) Illustration of valleys in the Brillouin zone and valley contrasting optical selection rules, for typical monolayer TMDs. (b) Bloch vector representation of valley DoF. Reprinted with permission from Hao *et al.*, Nat. Phys. **12**(7), 677–682 (2016). Copyright 2016 Springer Nature. (c) Illustration of valley polarization dynamics associated with excitons, inter-valley, and intra-valley trions in monolayer WSe_2. (c) Reprinted with permission Singh *et al.*, Phys. Rev. Lett. **117**(25), 257402 (2016). Copyright 2016 American Physical Society.

to link the quasiparticle and valley physics to optoelectronic devices based on TMDs.[79] Recently, Singh *et al.* have discovered exceptionally long valley polarization associated with intra-valley trions in monolayer WSe_2.[80]

Using a two-color pump/probe technique, systematic investigation of exciton and trion valley polarization dynamics is possible. The diagram shown in Fig. 4(c) captures current understanding of distinct exciton, inter-valley, and intra-valley trions dynamics in WSe_2.[80] The relevant resonances are arranged according to their energies. The top row diagrams correspond to the highest energy exciton resonance, the middle row diagrams represent the inter-valley trion $T_{|2\rangle}$, and the bottom row diagrams describe the intra-valley trions $T_{|1\rangle}$. When excitons are resonantly created, intrinsic electron-hole exchange interaction leads to rapid valley depolarization on time scales of ∼1 ps. Excitons can also capture an extra electron to form both types of trions, with a trion formation time of 1-2 ps depending on the density of free carriers. Following the resonant excitation of inter-valley trions $T_{|2\rangle}$, the most likely decay channel is to form $T_{|1\rangle}$ in the opposite valley, again due to electron-hole exchange interaction. The valley depolarization process of intra-valley trion $T_{|1\rangle}$ is rather unique. As illustrated toward the bottom of the diagram in Fig. 4(c), the transfer of either a single electron or an electron-hole pair to the other valley transforms the intra-valley trion into an inter-valley trion, which is an energetically unfavorable process. Scattering of K valley $T_{|1\rangle}$ to the opposite valley requires the simultaneous transfer of three carriers (two electrons and a hole) to the other valley, a restriction leading to a remarkably robust intra-valley trion polarization.

Another important aspect of quantum dynamics associated with the valley index is valley coherence time (or T_2 associated with the valley index). In particular, exciton and trion valley coherence times determine the time scale over which optical manipulation of the valley index via these optical transitions can be implemented. These important quantities have been directly measured experimentally using a nonlinear spectroscopy method, known as 2D Fourier transform spectroscopy.[81,82] These studies found that both exciton valley coherence and trion valley coherence are lost on ∼100-250 fs time scales. However, the decoherence mechanisms for exciton and trion valley coherence are distinct. It is likely that trion valley coherence may be significantly extended in high quality monolayer TMDs encapsulated between hBN layers.

B. Topology and correlation in monolayer WTe_2

The observation of the quantum spin Hall effect (QSHE) in time-reversal invariant 2D electronic systems has remained a milestone in the field of topological physics, as it has given rise to the notion of topological insulators (TI) and topological superconductors.[83,84] To date, there have been multiple predictions for the material realization of QSHE in a 2D TI. Such realizations can be classified into two categories: semiconductor heterostructures and monolayer crystals. Despite a decade of intense efforts, experimental evidence of this effect has been limited to a pair of semiconductor heterostructures (HgTe[85] and InAs/GaSb[86]) at temperatures close to that of liquid helium. Robust edge conductivity under broken time reversal symmetry is found in both systems—an unexpected behavior suggesting that the physics in these semiconductor heterostructures is beyond the simple quantum spin Hall (QSH) model.[86,87] Therefore, experimental realization of a new QSH system exhibiting the archetypical phenomenology and high temperature QSHE is highly desired.

Significant progress has recently been made in monolayer crystals. Since the first prediction in graphene,[88] a variety of atomically thin crystals have been predicted as 2D TIs, such as bismuth bilayer,[89–91] silicene,[92] gemanene,[92] stanene,[93] and so on. Monolayer TMDs have been predicted to have non-trivial topological characterization in their electronic states of the 1T′ lattice phase [Figs. 5(a) and 5(b)].[94] Analysis of the structural stability shows that S and Se compounds are more stable in the commonly found 2H phase, while Te compounds, especially WTe_2, prefer the 1T′ phase.

WTe_2 bulk is known to be a semimetal, and this property persists down to trilayer thicknesses [Fig. 5(c)].[95] However, different behaviors are observed in the mono- and bi-layers. It has been found that two probe conductance of mono- and bilayer WTe_2 has very strong gate dependence, close to zero gate voltages, and shows insulating behavior [Figs. 5(d) and 5(e)].[94] This observation suggests that a bandgap opens in mono- and bilayers of WTe_2. Strikingly, a residual conductance plateau (not quantized) is observed in the insulating region of the monolayer, but not the bilayer. This points to the

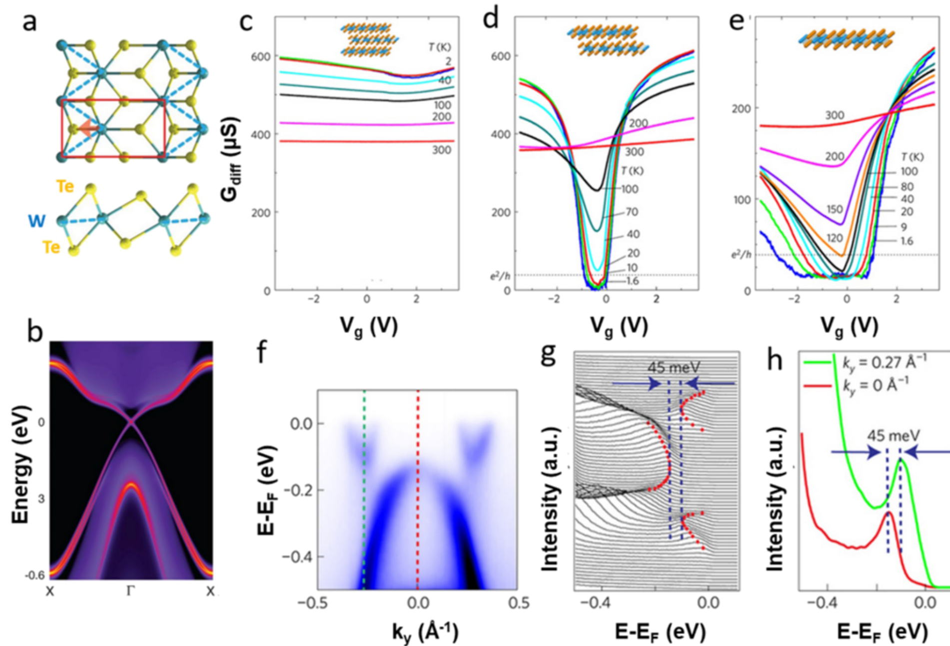

FIG. 5. Topological nature and bandgap opening in monolayer WTe_2. (a) Crystal structure (upper, top view; lower, side view). (b) The calculated band structure with the highlighted edge state near Γ point. [(c)–(e)] Gate dependence of the two-probe conductance taken at different temperatures, for trilayer, bilayer, and monolayer samples, respectively. (f) ARPES data of the monolayer with the K-doped surface. (g) The corresponding energy distribution curves (EDCs). (h) The two EDCs corresponding to the red and green lines in (f) highlighting the bandgap. Reprinted with permission from Fei *et al.*, Nat. Phys. **13**(7), 677–682 (2017). Copyright 2017 Nature Springer; Tang *et al.*, Nat. Phys. **13**(7), 683–687 (2017). Copyright 2017 Nature Springer; and Qian *et al.*, Science **346**(6215), 1344–1347 (2014). Copyright 2014 AAAS.[99]

predicted topological insulating nature of the monolayer, where the bulk is insulating and the edge is conducting. The work by Fei *et al.* confirmed that the residual conductance originates from the edge.[94] Independent studies[96,97] based on angle resolved photoemission spectroscopy (ARPES) and scanning tunneling spectroscopy (STS) draw the same conclusion. Figures 5(f) and 5(g) show the ARPES data taken from molecular beam epitaxy (MBE) grown monolayer WTe_2 and the corresponding energy distribution curves. A bandgap of about 45 meV is seen [Fig. 5(h)]. In the same study, the authors observed very different STS spectra between the monolayer interior and the edge, consistent with the prediction. The origin of the insulating gap at the mono- and bi-layer remains an open question and may be related to the strong electron correlation in the system.

The key to demonstrate the topological nature of the monolayer insulating state is to observe the quantized edge conductance (e^2/h per edge, where e is the elementary charge and h is Planck's constant), which is subsequently achieved by Wu *et al.*,[98] based on the innovation of the quantum device geometry. By combining multiple local bottom gates and a global top gate in the device shown in Figs. 6(a) and 6(b), the authors measured the intrinsic edge state resistance and performed length dependence studies. The resistance of short edge channels is found to be $\sim h/2 \times 10^2$ for two edges [Fig. 6(c)], corresponding to the Hallmark quantized value of QSHE. Another interesting observation is the appearance of the Dirac point in the edge band, as revealed by their magnetoresistance measurements. All these observations, together with theory, confirm that monolayer WTe_2 is a 2D TI, with a significantly larger bandgap compared to the semiconductor heterostructures. Indeed, Wu *et al.* found that the QSHE survives up to 100 K [Fig. 6(d)], which identifies monolayer WTe_2 as the first high temperature QSH system.

V. ELECTRONIC APPLICATIONS

2D materials are being explored for multiple electronic applications. However, and in order to make them technologically relevant, there is a need to explore their growth on a large scale. There is

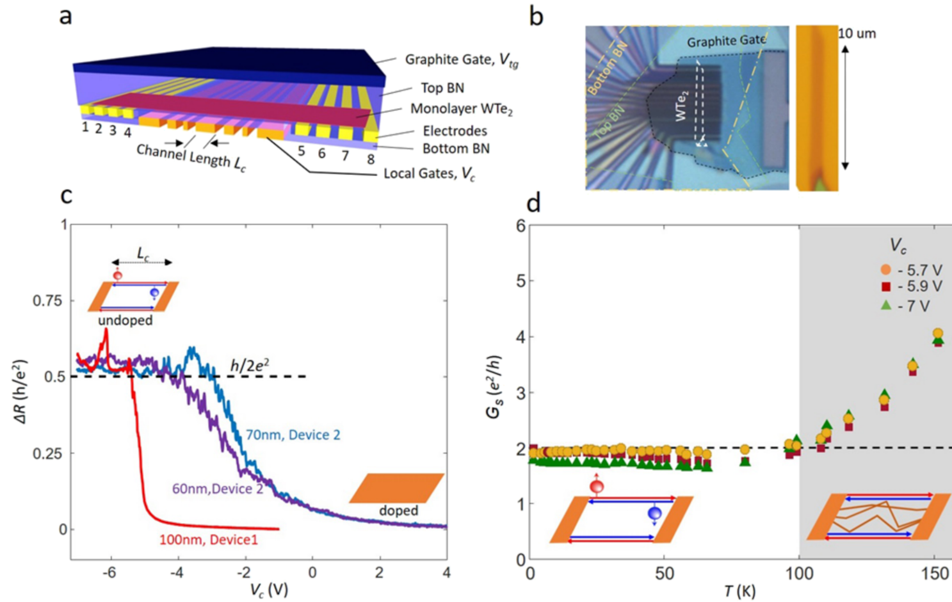

FIG. 6. Observation of the high temperature QSHE in monolayer WTe_2. (a) Device structures used by Wu *et al.*, which combine multiple local bottom gates and a global top gate. (b) The optical image of a typical device and the employed monolayer WTe_2. (c) The resistance of three edge channels (60 nm, 70 nm, and 100 nm in length, respectively) is near the quantum value of $h/2 \times 10^2$. (d) Temperature dependence of the channel conductance with a length of about 100 nm. The color of data indicates different gate voltages in the conductance plateau, namely, different Fermi levels at the edge band inside the bulk bandgap. Reprinted with permission from Wu *et al.*, Science **359**(6371), 76–79 (2018). Copyright 2018 AAAS.

also a need to study proof-of-concept electronic properties and make an attempt to translate these to technologically relevant scales. Here, we explore some non-conventional (non-transistor) electronic applications of 2D materials.

A. Atomic membranes for straintronics

2D crystals are known to possess many desirable mechanical properties, such as extreme stiffness, flexibility, and the ability to withstand very high strains before rupture.[100,101] Studies have shown that the band structures of many 2D crystals are highly sensitive to strain. Strain has been found to reduce the bandgap energy of many of the TMDs including MoS_2,[39,102–105] $MoSe_2$,[106] $MoTe_2$,[107] WS_2,[108] and WSe_2.[109] Strain sensitivities of the bandgaps in these materials can be as high as ∼50 meV/% for uniaxial strain and ∼100 meV/% biaxial strain.[110] Strain has also been shown to influence optical properties such as the emission and absorption spectrum[102] as well as the photoluminescence (PL) polarization[111] of TMDs, and very high local strains in graphene nanobubbles are found to induce pseudo-magnetic fields which strongly affect the behavior of electrons within the strained area.[112] These various strain effects may be used as a way to enhance the electrical and optical properties of existing 2D optoelectronic applications, or be used as a basis on which to build novel electronic devices.[113,114] 2D materials can also be used to make highly sensitive measurements of strain or pressure, and an MoS_2 strain sensor was recently found to have a strain gauge comparable to that of a state of the art silicon sensor.[115]

A number of techniques have emerged for introducing strain into 2D crystals; however, the most widely used geometry involves placing the crystal on a flexible substrate which is then stretched or bent [Fig. 7(a)].[102,104,108,109,111,116,117] Strain can also be introduced by draping membranes over corrugated surfaces,[118] using Micro-Electro-Mechanical System (MEMS) mechanical actuators,[119,120] by nanoindentation of suspended membranes [Fig. 7(b)][115] or by producing wrinkles with highly localized regions of strain [Fig. 7(c)].[39] Another technique involved suspending MoS_2 membranes over cylindrical cavities and applying a pressure difference to deform them [Fig. 7(d)].[110] This deformation produced uniaxial strain at the edge of the bulge and biaxial strain at the center. Larger pressure

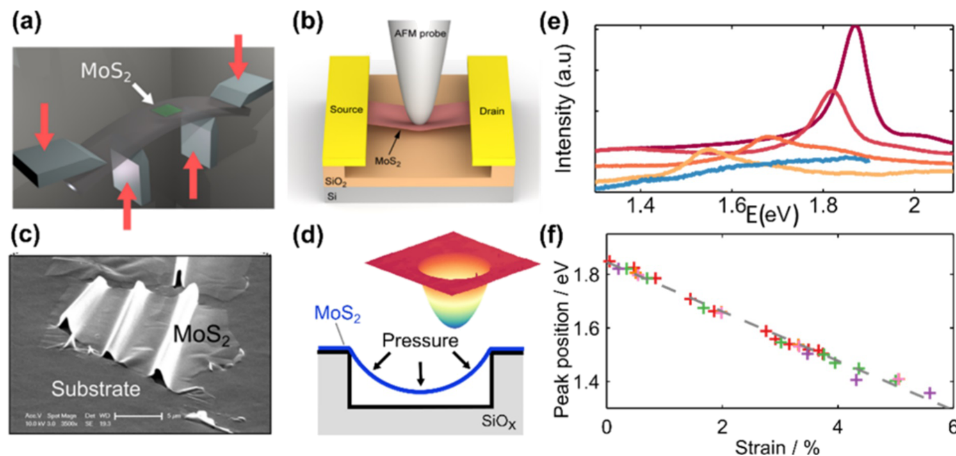

FIG. 7. (a) Four-point bending apparatus for inducing uniaxial strain. Reprinted with permission from Conley *et al.*, Nano Lett. **13**(8), 3626–3630 (2013). Copyright 2013 American Chemical Society. (b) A membrane connected to electrical contacts and suspended over a trench. Strain is introduced via nanoindentation, allowing one to measure strain induced changes to the electrical current across the device. Reprinted with permission from Manzeli et al., Nano Lett. 15(8), 5330–5335 (2015). Copyright 2015 American Chemical Society. (c) Wrinkled MoS_2 on a polymer substrate containing highly localized regions of strain. Reprinted with permission from Castellanos-Gomez *et al.*, Nano Lett. **13**(11), 5361–5366 (2013). Copyright 2013 American Chemical Society. (d) A membrane suspended over a microcavity and deformed by an applied external pressure. Biaxial strain is produced in the center of the bulge. (e) The effect of biaxial strain on the PL spectrum of monolayer MoS_2. At over 5% strain, the PL peak is reduced to 1.4 eV. (f) The MoS_2 PL peak position as a function of biaxial strain. (d)–(f) are reprinted with permission from Lloyd *et al.*, Nano Lett. **16**(9), 5836–5841 (2016). Copyright 2016 American Chemical Society.

differences produced larger strains, the magnitude of which could be measured with an atomic force microscope (AFM).

Figure 7(e) shows the PL spectra of a monolayer device over the range of 0%-5.6% biaxial strain. As the biaxial strain is increased, the PL peak red shifts from an initial energy of ~1.9 eV to a final energy of ~1.4 eV. In this manner, the authors deduced that the strain shift rate of the MoS_2 optical bandgap was 105 meV/% [Fig. 7(f)]. The data amassed so far shows that many 2D materials are electrically and optically sensitive to strain and can also withstand high strains before rupturing. These data also point to situations where strain should be desirable or avoided. As can be seen from Fig. 7(e), the emission intensity of the MoS_2 PL peak is significantly reduced when large biaxial strains are applied due to strain causing the bandgap to transition from direct to indirect in nature. By contrast, Desai *et al.* found that uniaxial tensile strain caused multilayer WSe_2 to transition from being an indirect to a direct semiconductor.[109] For devices which require direct bandgaps, such as in light-emitting diodes (LEDs) or photodetectors, strain can therefore enhance or degrade device performance depending on the material.

Despite the success of these studies, straintronic devices often experience a limitation in the magnitude of the strain which can be applied before slipping occurs. This happens when the frictional forces between the crystal and substrate can no longer equal the tensile forces within the membrane. One solution to slipping could be to pin the edges of the crystal on a high adhesion surface such as gold[121] or using a top metal "clamp."[107] Additionally, 2D membranes can fracture as a result of nano-indentation. While 2D materials have shown large intrinsic strengths, CVD membranes exhibit defects, cracks, and grain boundaries which strongly affect the fracture stress of the material. The crystal quality in samples is therefore important for reaching high strains.

B. 2D low power electronics

Scaling of conventional metal oxide semiconductor field effect transistors (MOSFETs) based on silicon is nearing the end of its evolutionary path owing to fundamental limitations at the material and device physics levels.[122] 2D materials are good alternatives because they not only allow aggressive dimension scaling due to their few-atom thickness but also offer novel physics which could reduce operating voltages.[123,124] (Power dissipation during digital operation scales as voltage squared.)

A fundamental limitation of MOSFETs based on silicon or any other materials is that their "turn-on" is limited by thermionic emission and the Boltzmann tail of the electron (or hole) distribution to 60 mV/decade at room temperature. More energy-efficient transistor switches should turn on with a "steeper" subthreshold swing (SS) closer to zero, i.e., over an order of magnitude jump in current with less than 60 mV increase in gate voltage.

To avoid the thermionic operating limitations of MOSFETs, in recent years progress has been made toward the so-called steep-slope tunneling field effect transistors (TFETs) based on 2D materials.[123,128–130] TFETs operate by quantum mechanical tunneling of electrons from the valence to the conduction band of the channel, with the band bending controlled by the gate [Fig. 8(a)], and thereby allow sub-60 mV/decade SS at room temperature. However, TFETs suffer from low ON current owing to lower transmission probability through the semiconductor bandgap, which could be compensated by the ultra-thin nature of 2D materials which reduces the tunneling distance. Sarkar *et al.*[130] demonstrated steep turn-on with minimum SS ≈ 3.9 mV/decade and an average SS ≈ 31.1 mV/decade over four decades of drain current at room temperature, in an atomically thin and layered semiconducting-channel tunnel-FET (ATLAS-TFET) by using highly doped Ge as the source and bilayer MoS_2 as the channel.

Furthermore, various groups have demonstrated steep-slope negative capacitance field effect transistors (NCFETs), by integrating hafnium zirconium oxide ($HfZrO_2$ or HZO) ferroelectric into the gate stack of a MoS_2 2D-FET.[131–133] The original NCFET idea was proposed by Salahuddin and

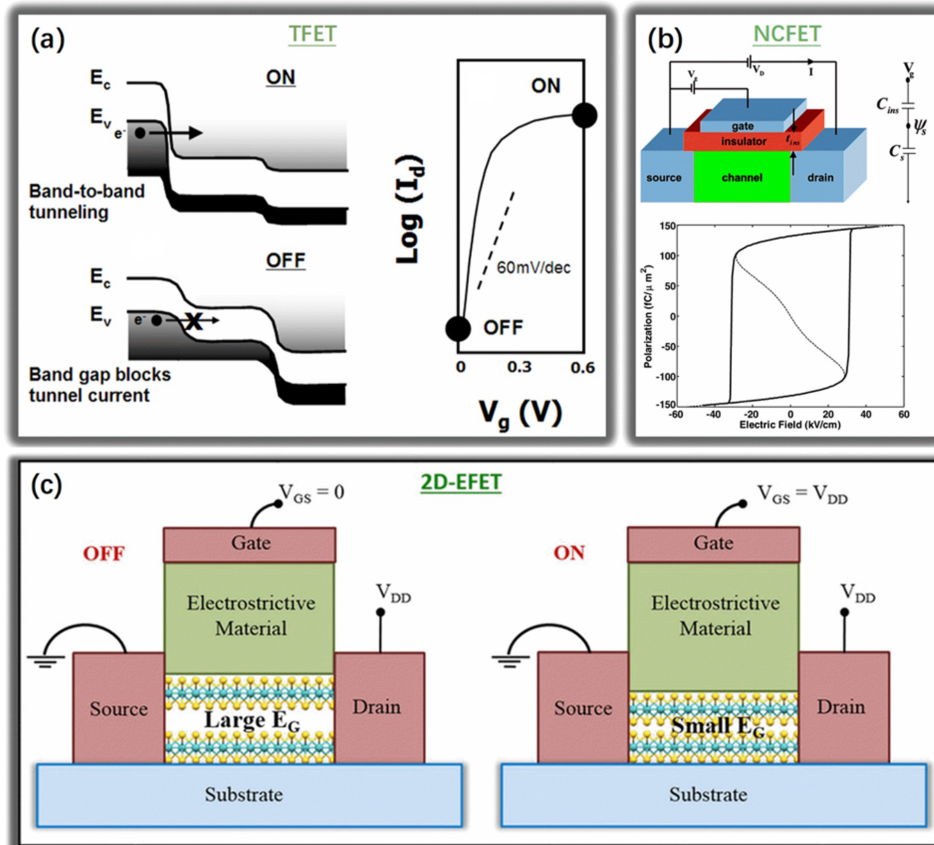

FIG. 8. Principles of operation for (a) TFET, (b) NCFET, and (c) 2D EFET. (a) Reprinted with permission from Kim *et al.*, "Low power circuit design based on heterojunction tunneling transistors (HETTs)," in *ACM/IEEE International Symposium on Low-Power Electronics Design* (Association for Computing Machinery, New York, 2009). Copyright 2009 Association for Computing Machinery, Inc.[125] (b) Reprinted with permission from S. Salahuddin and S. Datta, Nano Lett. **8**(2), 405–410 (2008). Copyright 2008 American Chemical Society. (c) Reprinted with permission from S. Das, Sci. Rep. **6**, 34811 (2016). Copyright 2016 Springer Nature.

Datta,[126] where the steep SS was achieved by utilizing the inherent negative slope of the polarization versus electric field characteristic (P-E) of a ferroelectric insulator that results in negative capacitance as shown in Fig. 8(b). Ordinarily the negative slope segment is unstable and obscured by the hysteretic jumps in the polarization. However, by placing the ferroelectric capacitor in series with a normal capacitor, for example, the channel capacitance of a FET, the negative capacitance can be manifested which in turn provides a voltage amplification at the internal node. This allows the channel surface potential to exceed the applied gate potential and overcome the Boltzmann limit, thus enabling sub-60 mV/decade steep SS.

In addition, Das *et al.*[127] proposed a new device concept with sub-60 mV/decade SS at room temperature, referred to as 2D electrostrictive field effect transistor (2D-EFET). This combines the aggressive dimension scalability of 2D materials with their stress-induced dynamic bandgap engineering. The device structure relies on a 2D semiconductor transistor channel, with the gate insulator being replaced by an electrostrictive or piezoelectric ceramic as shown in Fig. 8(c). In the absence of any applied gate bias (i.e., OFF state), the 2D channel offers a sizeable bandgap (∼1-2 eV) and prevents current conduction between the source and the drain. However, when a finite gate bias is applied across the electrostrictive material (i.e., ON state), it undergoes longitudinal expansion and transduces an out-of-the-plane stress on the 2D channel and thereby reduces the bandgap of the 2D material. This allows current conduction between the source and the drain. Moreover, such stress-induced dynamic bandgap engineering leads to internal voltage amplification, resulting in sub-60 mV/decade steep switching at room temperature. A similar idea was proposed by IBM researchers based on vertical integration of the piezoresistive material with the piezoelectric material.[134] In addition to the development and demonstration of multiple novel beyond Boltzmann device concepts, a significant amount of research effort is also being invested toward 2D neuromorphic devices for low power computing.[135–137]

C. Power dissipation in 2D electronics

Emerging electronic applications of 2D materials include multi-layer processors monolithically integrated with memory,[138] and wearable electronics which require integration with poor thermal substrates such as flexible plastics.[139] It is known that power dissipation has been a major bottleneck in the performance of ICs for over a decade,[140] and this could become an even greater challenge in such 2D devices and systems, due to poor thermal conductivities and a large number of thermal interfaces. Fundamentally, the power in 2D electronics is dissipated via electron-phonon interactions in the ultra-thin (∼0.6 nm) transistor channel[140] and at its contacts. The generated heat can "escape" via the substrate in most cases[141] or via the contacts in sub-100 nm devices.[142] The gate primarily acts as a thermal capacitor limiting the thermal time constant of the device and playing a greater role in transient (e.g., pulsed) rather than steady-state operation.[143] Today's electrical contacts are considered to limit the performance of sub-100 nm 2D transistors,[144] but even ideal contacts may be expected to affect power dissipation via thermoelectric effects in highly scaled devices.[145]

Here we focus on understanding the power dissipation in 2D transistor channels, where the heat flows across the interface and to surrounding insulators, after which it dissipates into the substrate. Due to the ultra-thin, sub-nm nature of the material, thermal interfaces dominate the overall thermal resistance of such devices. One of the key challenges in the measurement of these thermal interfaces is the need to differentiate the temperature of the 2D material from its surrounding. In this context, the material selectivity of Raman spectroscopy holds a unique advantage as the temperature of even a monolayer semiconductor can be distinguished from the material directly under (or above) it, if the Raman signatures are distinct.[141,146] Basic predictions can be made by modeling the self-heating in the transistor as described in Ref. 142. The model includes the thermal resistance R_{TH} of the device such that the temperature rise is $\Delta T = PR_{TH}$, where P is the power input of the device. In devices longer than the lateral thermal healing length ($L_H \approx 100$ nm for 1L MoS_2 on 90 nm SiO_2 on Si),[141,142] the total thermal resistance can be divided into three main components: the thermal boundary resistance (TBR) between the 2D channel and the supporting oxide, the spreading thermal resistance of the bottom oxide ($\mathcal{R}_{BOX}$), and the spreading thermal resistance into the substrate ($\mathcal{R}_{Si}$), as shown in Fig. 9(a).[142] The electrical behavior (drain current *vs.* voltage) of a MoS_2 transistor with different thermal surroundings is simulated in Fig. 9(b). The drastic reduction in saturation current

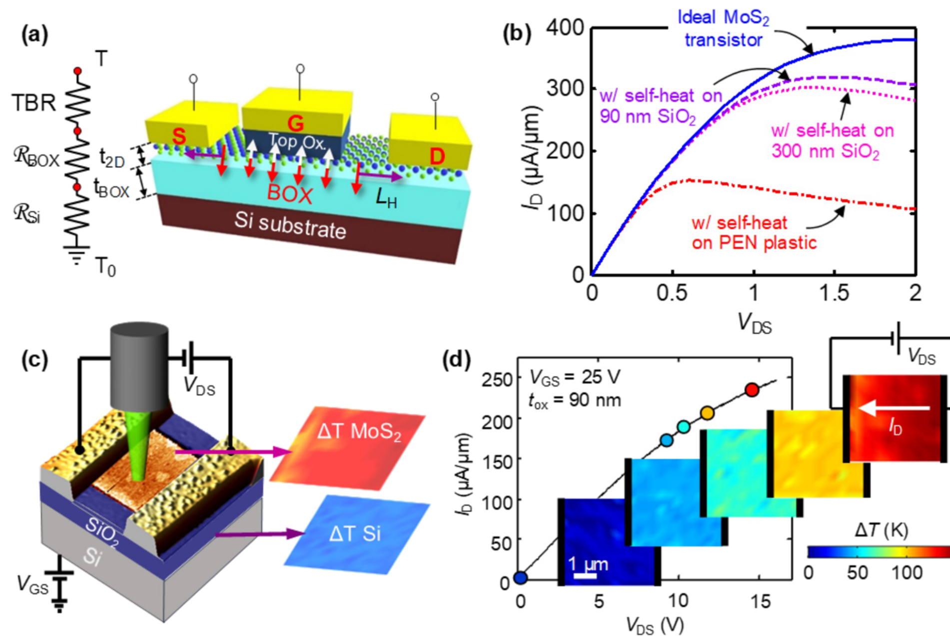

FIG. 9. Power dissipation in 2D electronics. (a) Schematic of thermal model of 2D transistor. Arrows show the direction of heat flow: in most cases to the substrate (red), via the contacts in sub-100 nm devices (purple), and transient heat flow to the top gate (white). (b) Simulated I_D *vs.* V_{DS} for an "ideal" 1L MoS_2 FET ($L = 1\ \mu$m) without self-heating (solid line, top curve), with self-heating on 90 nm SiO_2 on the Si substrate (dashed), with self-heating on 300 nm SiO_2 on Si substrate (dotted), and on a poor thermal substrate where the Si was replaced by a polymer (dashed-dotted).[142] [(a) and (b)] Reprinted with permission from S. V. Suryavanshi and E. Pop, J. Appl. Phys. **120**(22), 224503 (2016). Copyright 2016 American Institute of Physics. (c) Raman thermometry measurement of temperature rise in functioning MoS_2 FET.[141] Temperature maps of the MoS_2 channel and the Si surface directly underneath are obtained simultaneously. (d) Measured I_D *vs.* V_{DS} and corresponding temperature maps. Colored circles mark the bias point of each temperature color map. The white arrow shows the current flow direction. The thermal boundary conductance (resistance) of the MoS_2-SiO_2 interface is estimated to be TBC ≈ 14 MW m^{-2} K^{-1} (TBR ≈ 70 m^2 K/GW), equivalent to a relatively large Kapitza length, L_K ≈ 100 nm of SiO_2. [(c) and (d)] Reprinted with permission from Yalon *et al.*, Nano Lett. **17**(6), 3429–3433 (2017). Copyright 2017 American Chemical Society.

by ∼25% on SiO_2/Si and ∼70% on plastic substrates highlights the crucial role of self-heating, especially in devices with high current density (>0.25 mA/μm), as were recently demonstrated for MoS_2.[131,147,148]

The role of the thermal interface, namely, the TBR can be understood by comparing it to the characteristic Kapitza length L_K that is the equivalent thickness of a material with the same thermal resistance. For example, in SiO_2: $L_K = k_{ox}\cdot$TBR, where k_{ox} is the thermal conductivity of SiO_2. Raman thermometry and scanning thermal microscopy (SThM) were utilized to experimentally measure the TBR of the MoS_2-SiO_2 interface and to uncover power dissipation in 2D semiconductor transistors.[141] Figure 9(c) shows the schematic device structure and measurement setup. The Raman signal was measured while electrical bias is applied and converted to temperature rise via calibration on a hot stage.[141] The material selectivity of the Raman technique enables simultaneous temperature maps of the MoS_2 channel and the Si substrate underneath it [Fig. 9(c)]. Figure 9(d) displays temperature maps of the MoS_2 channel at varying power inputs, shown as colored circles on the output characteristics. Interestingly, the obtained temperature maps are uniform despite small bilayer (2L) islands present in the material grown by chemical vapor deposition[149] which are visible in the topography map in Fig. 9(c). The uniform heating implies that such 2D semiconductors are less sensitive to inhomogeneity than expected, which is a result of the conduction band energy difference between 1L and 2L being small, of the order ∼50 meV.[150,151] In addition, the differential Raman measurement reveals TBR ≈ 70 m^2 K/GW (or thermal boundary conductance, TBC ≈ 14 MW m^{-2} K^{-1}) at the MoS_2-SiO_2 interface.[141,152] This TBR is equivalent to a Kapitza length L_K ∼ 100 nm SiO_2, and it is relatively large compared to most known solid-solid interfaces.[140,153] These results suggest that the thermal interfaces of 2D semiconductors will ultimately limit their energy dissipation. Such 2D

electronics can nonetheless benefit from better heat sinking substrates, while poor thermal substrates like flexible plastics could severely limit their performance. We also note that partial device cooling could be obtained from capping layers with higher thermal conductivity (e.g., h-BN), in short-channel devices (<100 nm)[147] where partial heat sinking can occur directly to the contacts.[95]

D. 2D Cu diffusion barriers for ultra-scaled interconnect technology

Typical IC chips consist of both transistors and interconnects. The former is referred to as the front-end-of-line (FEOL), whereas the latter is known as the back-end-of-line (BEOL). While significant efforts have been made to improve the performance and to reduce the size of transistors, interconnects are often the performance bottleneck as their resistive-capacitive (RC) delay starts to dominate the total delay of the entire chip, causing any FEOL advancements to be reduced by the BEOL. Copper (Cu) has been used as the interconnect material because of its superior conductivity. However, Cu also has a high atomic diffusivity, which leads to reliability challenges as interconnects are reduced in size. On one hand, when Cu atoms or ions diffuse through the dielectric used to isolate interconnects, different interconnects will be shorted, leading to chip failure. On the other hand, if Cu diffuses into transistors it can introduce deep-level traps and affect their performance. Conventional materials, such as Ta/TaN and TiN, have been used as barriers surrounding Cu interconnects, to block the outdiffusion of Cu atoms. Because barrier materials are more resistive than Cu, as the dimensions of interconnect are reduced, the thicknesses of diffusion barriers should also be reduced to ensure overall low resistivity of the entire wire (Cu and barrier). However, these conventional barrier materials can no longer block Cu diffusion when their thicknesses are aggressively scaled, as shown in the left part of Fig. 9(a). The International Technology Roadmap for Semiconductors (ITRS)[154] suggests that the thickness requirement of the diffusion barrier would be 1 nm by the year 2021.

2D materials can naturally satisfy the sub-1 nm requirement due to their ultra-thin body thicknesses. In addition, graphene was found to enhance the electrical and thermal conductivity of Cu nanowires.[155] Therefore, it is essential to investigate 2D materials' ability to block Cu diffusion and determine whether they can be used as diffusion barrier alternatives. One of the common approaches to evaluate diffusion barriers is time-dependent dielectric breakdown (TDDB) measurement.[156–160] In the TDDB measurement setup, shown in the right-hand side of Fig. 9(a), a positive constant voltage is applied on the Cu electrode of a capacitor structure, while the Si substrate is grounded. In this way, a constant electric field is created across the dielectric layer, which can drive Cu ions into the dielectric beneath the Cu electrode.[161] The presence of Cu atoms or ions in the dielectric can lead to an early device breakdown due to the formation of a conductive path and/or the assistance in Poole-Frenkel tunneling.[159] The 2D material for evaluation was prepared on the top of the dielectric, followed by the deposition of Cu electrodes. If the 2D material can successfully mitigate Cu diffusion, the device breakdown time will be extended.

Figure 10(b) shows a representative device comparison with and without three-to-four-layer (3-4L, ~0.99-1.32 nm) hexagonal boron nitride (h-BN). The h-BN film was grown by CVD on Cu foils and then transferred onto a SiO_2/Si substrate. It is clear that the device breakdown time is much longer with the presence of the h-BN. In addition, MoS_2 was also evaluated. The predominantly 1L MoS_2 film (~0.615 nm thick) was directly grown on a SiO_2 substrate by CVD at 850 °C.[149] Time-to-breakdown (t_{BD}) of multiple devices was recorded and used to plot the statistics in Figs. 10(c) and 10(d). At a certain electric field, the device with the shortest/longest t_{BD} was assigned to have the lowest/highest value of the cumulative probability, and median-time-to-failure ($TTF_{50\%}$) can be extracted as an indication of the extent of Cu ion diffusion. This TDDB plot provides a statistical evaluation of the dielectric quality that is affected by Cu ion diffusion. As can be observed, t_{BD} of devices with h-BN and MoS_2 barriers increases in general. Furthermore, TDDB measurements at various electric fields were conducted. After acquiring $TTF_{50\%}$ at various fields, the lifetime under normal operating conditions (much lower electric fields) can be extrapolated using various models, such us E-model, 1/E-model, and sqrt-E-model. Figures 10(e) and 10(f) show the lifetime prediction of devices with h-BN and MoS_2, compared to their control samples. From the E-model, the lifetime of devices with 3-4L h-BN and 1L MoS_2 at 0.5 MV/cm is 7.5×10^6 s and

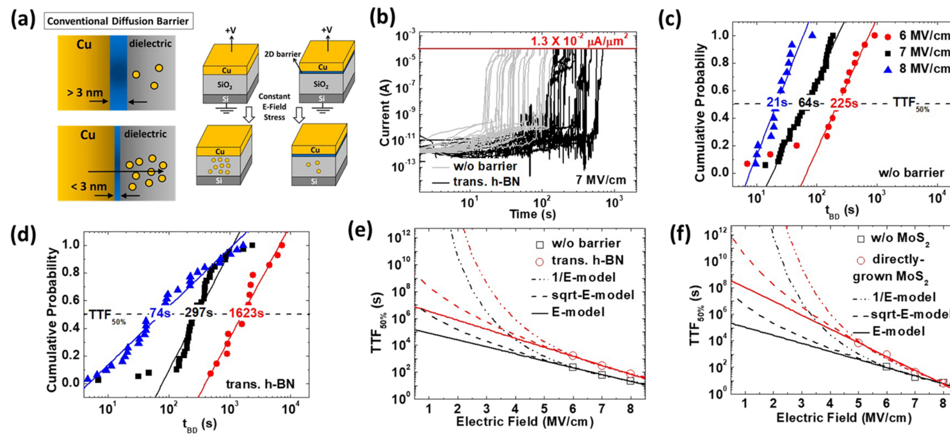

FIG. 10. (a) Illustration of the inability of conventional barrier materials to block Cu ion diffusion when they are ultra-scaled (left) and schematic of TDDB measurement on a capacitor structure (right). (b) Current evolution with stress time at a constant electric field of 7 MV/cm. [(c) and (d)] TDDB results of devices (c) without barrier and (d) with h-BN barrier at various electric fields. [(e) and (f)] Lifetime prediction using various models and the comparison of devices without barriers and with (e) h-BN or (f) MoS_2 as a Cu diffusion barrier. [(b)–(f)] Reprinted with permission from Lo *et al.*, npj 2D Mater. Appl. **1**, 42 (2017). Copyright 2017 Springer Nature.

3.7×10^8 s, respectively ($\sim 2 \times 105$ s for devices without barriers). Detailed discussions can be found in Refs. 162 and 163.

VI. CONCLUSION AND PERSPECTIVE

This article highlights a number of studies on 2D materials that include synthesis, defect engineering, physical properties, and electronic applications. It provides insight into the current directions of 2D materials research and discusses areas which require further investigation.

The field of 2D materials remains a rapidly evolving and fruitful area of research. With tremendous progress in the application of 2D materials, fundamental scientific research is still needed, particularly in relation to materials growth and defect characterization, as well as fundamental physical phenomena of 2D materials. Beyond these areas, progress has been made in 2D materials for many valuable electronic applications including flexible electronics and diffusion barriers. Furthermore, continued device-motivated studies serve to further understand functional device requirements such as those related to power dissipation. Over a decade after its inception, this exciting area of research continues to advance, with studies constantly pushing the boundaries of the field—from the realization of new 2D materials to their exotic properties and increasingly many applications. There are many open-ended questions in this field, stemming from two major aspects—industry and academia. The industrial aspect of 2D materials is focused on standardization of these materials in order to be able to benchmark them as has been done for other commercially available materials. There is a lot of development taking place with university-industry partnerships with the focus of establishing techniques for large scale growth of 2D materials and quality assessment. From an academic standpoint, there is emerging interest in biomedical applications of TMDs including biosensing, bioimaging, and therapy.[8] Recent advancements in material synthesis and encapsulations have also created unprecedented opportunities to explore superconductivity and magnetism at the 2D limit.[164,165] These open-ended questions will lead to fruitful research in fundamental properties and practical applications of 2D materials in the future.

ACKNOWLEDGMENTS

This review article was based on contents discussed in the 5th annual Graphene and Beyond workshop held at Pennsylvania State University. The workshop was sponsored by Corning, Morgan Advanced Materials, APL Materials, CVD Equipment Corporation, and FEI. The authors thank the

following funding agencies for supporting their research: NSF, DOE, DOD, AFOSR, and SRC. The authors also thank NEWLIMITS, a center in nCORE, a Semiconductor Research Corporation (SRC) program sponsored by NIST and thank LEAST, one of six STARnet Centers, a SRC program sponsored by MARCO and DARPA.

[1] K. S. Novoselov, A. K. Geim, S. V. Morozov, D. Jiang, Y. Zhang, S. V. Dubonos, I. V. Grigorieva, and A. A. Firsov, Science **306**(5696), 666–669 (2004).
[2] C. L. Tan, X. H. Cao, X. J. Wu, Q. Y. He, J. Yang, X. Zhang, J. Z. Chen, W. Zhao, S. K. Han, G. H. Nam, M. Sindoro, and H. Zhang, Chem. Rev. **117**(9), 6225–6331 (2017).
[3] R. Roldan, L. Chirolli, E. Prada, J. A. Silva-Guillen, P. San-Jose, and F. Guinea, Chem. Soc. Rev. **46**(15), 4387–4399 (2017).
[4] J. R. Schaibley, H. Y. Yu, G. Clark, P. Rivera, J. S. Ross, K. L. Seyler, W. Yao, and X. D. Xu, Nat. Rev. Mater. **1**(11), 16055 (2016).
[5] K. F. Mak and J. Shan, Nat. Photonics **10**(4), 216–226 (2016).
[6] H. Jin, C. Guo, X. Liu, J. Liu, A. Vasileff, Y. Jiao, Y. Zheng, and S.-Z. Qiao, Chem. Rev. **118**, 6337 (2018).
[7] E. Pomerantseva and Y. Gogotsi, Nat. Energy **2**(7), 17089 (2017).
[8] X. Li, J. Y. Shan, W. Z. Zhang, S. Su, L. H. Yuwen, and L. H. Wang, Small **13**(5), 1602660 (2017).
[9] H. Li, Y. Li, A. Aljarb, Y. Shi, and L.-J. Li, Chem. Rev. **118**, 6134 (2017).
[10] Z. H. Hu, Z. T. Wu, C. Han, J. He, Z. H. Ni, and W. Chen, Chem. Soc. Rev. **47**(9), 3100–3128 (2018).
[11] Z. Lin, B. R. Carvalho, E. Kahn, R. T. Lv, R. Rao, H. Terrones, M. A. Pimenta, and M. Terrones, 2D Mater. **3**(2), 022002 (2016).
[12] A. K. Geim and I. V. Grigorieva, Nature **499**(7459), 419–425 (2013).
[13] S. Manzeli, D. Ovchinnikov, D. Pasquier, O. V. Yazyev, and A. Kis, Nat. Rev. Mater. **2**(8), 17033 (2017).
[14] S. Z. Butler, S. M. Hollen, L. Cao, Y. Cui, J. A. Gupta, H. R. Gutierrez, T. F. Heinz, S. S. Hong, J. Huang, A. F. Ismach, E. Johnston-Halperin, M. Kuno, V. V. Plashnitsa, R. D. Robinson, R. S. Ruoff, S. Salahuddin, J. Shan, L. Shi, M. G. Spencer, M. Terrones, W. Windl, and J. E. Goldberger, ACS Nano **7**(4), 2898–2926 (2013).
[15] G. R. Bhimanapati, Z. Lin, V. Meunier, Y. Jung, J. Cha, S. Das, D. Xiao, Y. Son, M. S. Strano, V. R. Cooper, L. Liang, S. G. Louie, E. Ringe, W. Zhou, S. S. Kim, R. R. Naik, B. G. Sumpter, H. Terrones, F. Xia, Y. Wang, J. Zhu, D. Akinwande, N. Alem, J. A. Schuller, R. E. Schaak, M. Terrones, and J. A. Robinson, ACS Nano **9**(12), 11509–11539 (2015).
[16] A. J. Mannix, B. Kiraly, M. C. Hersam, and N. P. Guisinger, Nat. Rev. Chem. **1**(2), 0014 (2017).
[17] K. K. H. Smithe, S. V. Suryavanshi, M. M. Rojo, A. D. Tedjarati, and E. Pop, ACS Nano **11**(8), 8456–8463 (2017).
[18] Y. J. Zhan, Z. Liu, S. Najmaei, P. M. Ajayan, and J. Lou, Small **8**(7), 966–971 (2012).
[19] Y. H. Lee, X. Q. Zhang, W. J. Zhang, M. T. Chang, C. T. Lin, K. D. Chang, Y. C. Yu, J. T. W. Wang, C. S. Chang, L. J. Li, and T. W. Lin, Adv. Mater. **24**(17), 2320–2325 (2012).
[20] K. Kang, S. E. Xie, L. J. Huang, Y. M. Han, P. Y. Huang, K. F. Mak, C. J. Kim, D. Muller, and J. Park, Nature **520**(7549), 656–660 (2015).
[21] Y. Sun, Y. Wang, D. Sun, B. R. Carvalho, C. G. Read, C. H. Lee, Z. Lin, K. Fujisawa, J. A. Robinson, V. H. Crespi, M. Terrones, and R. E. Schaak, Angew. Chem., Int. Ed. **55**(8), 2830–2834 (2016).
[22] V. Nicolosi, M. Chhowalla, M. G. Kanatzidis, M. S. Strano, and J. N. Coleman, Science **340**(6139), 1226419 (2013).
[23] K. K. Liu, W. J. Zhang, Y. H. Lee, Y. C. Lin, M. T. Chang, C. Su, C. S. Chang, H. Li, Y. M. Shi, H. Zhang, C. S. Lai, and L. J. Li, Nano Lett. **12**(3), 1538–1544 (2012).
[24] Y. Lei, S. Pakhira, K. Fujisawa, X. Wang, O. O. Iyiola, N. Perea López, A. Laura Elías, L. Pulickal Rajukumar, C. Zhou, and B. Kabius, ACS Nano **11**, 5103–5112 (2017).
[25] S. Das, M. K. Bera, S. Tong, B. Narayanan, G. Kamath, A. Mane, A. P. Paulikas, M. R. Antonio, S. K. Sankaranarayanan, and A. K. Roelofs, Sci. Rep. **6**, 28195 (2016).
[26] J. Deng, H. Li, J. Xiao, Y. Tu, D. Deng, H. Yang, H. Tian, J. Li, P. Ren, and X. Bao, Energy Environ. Sci. **8**(5), 1594–1601 (2015).
[27] V. Kiran, D. Mukherjee, R. N. Jenjeti, and S. Sampath, Nanoscale **6**(21), 12856–12863 (2014).
[28] S. Mouri, Y. Miyauchi, and K. Matsuda, Nano Lett. **13**(12), 5944–5948 (2013).
[29] Y. Gong, Z. Liu, A. R. Lupini, G. Shi, J. Lin, S. Najmaei, Z. Lin, A. L. Elias, A. Berkdemir, G. You, H. Terrones, M. Terrones, R. Vajtai, S. T. Pantelides, S. J. Pennycook, J. Lou, W. Zhou, and P. M. Ajayan, Nano Lett. **14**(2), 442–449 (2014).
[30] M. Zhang, J. Wu, Y. Zhu, D. O. Dumcenco, J. Hong, N. Mao, S. Deng, Y. Chen, Y. Yang, C. Jin, S. H. Chaki, Y. S. Huang, J. Zhang, and L. Xie, ACS Nano **8**(7), 7130–7137 (2014).
[31] Y. Chen, J. Xi, D. O. Dumcenco, Z. Liu, K. Suenaga, D. Wang, Z. Shuai, Y. S. Huang, and L. Xie, ACS Nano **7**(5), 4610–4616 (2013).
[32] J. Mann, Q. Ma, P. M. Odenthal, M. Isarraraz, D. Le, E. Preciado, D. Barroso, K. Yamaguchi, G. von Son Palacio, and A. Nguyen, Adv. Mater. **26**(9), 1399–1404 (2014).
[33] J. Suh, T. E. Park, D. Y. Lin, D. Fu, J. Park, H. J. Jung, Y. Chen, C. Ko, C. Jang, Y. Sun, R. Sinclair, J. Chang, S. Tongay, and J. Wu, Nano Lett. **14**(12), 6976–6982 (2014).
[34] L. Yang, K. Majumdar, H. Liu, Y. Du, H. Wu, M. Hatzistergos, P. Y. Hung, R. Tieckelmann, W. Tsai, C. Hobbs, and P. D. Ye, Nano Lett. **14**(11), 6275–6280 (2014).
[35] Z. Lin, M. T. Thee, A. L. Elias, S. M. Feng, C. J. Zhou, K. Fujisawa, N. Perea-Lopez, V. Carozo, H. Terrones, and M. Terrones, APL Mater. **2**(9), 092514 (2014).
[36] S. Zheng, L. Sun, T. Yin, A. M. Dubrovkin, F. Liu, Z. Liu, Z. X. Shen, and H. J. Fan, Appl. Phys. Lett. **106**(6), 063113 (2015).
[37] A. Azizi, Y. Wang, Z. Lin, K. Wang, A. L. Elias, M. Terrones, V. H. Crespi, and N. Alem, Nano Lett. **16**(11), 6982–6987 (2016).

[38] A. Kushima, X. Qian, P. Zhao, S. Zhang, and J. Li, Nano Lett. **15**(2), 1302–1308 (2015).
[39] A. Castellanos-Gomez, R. Roldan, E. Cappelluti, M. Buscema, F. Guinea, H. S. van der Zant, and G. A. Steele, Nano Lett. **13**(11), 5361–5366 (2013).
[40] A. Ostadhossein, A. Rahnamoun, Y. Wang, P. Zhao, S. Zhang, V. H. Crespi, and A. C. van Duin, J. Phys. Chem. Lett. **8**(3), 631–640 (2017).
[41] K. N. Kudin, G. E. Scuseria, and B. I. Yakobson, Phys. Rev. B **64**(23), 235406 (2001).
[42] K. A. Zhang and M. Arroyo, J. Mech. Phys. Solids **72**, 61–74 (2014).
[43] C. K. Oliveira, E. F. A. Gomes, M. C. Prado, T. V. Alencar, R. Nascimento, L. M. Malard, R. J. C. Batista, A. B. de Oliveira, H. Chacham, A. M. de Paula, and B. R. A. Neves, Nano Res. **8**(5), 1680–1688 (2015).
[44] Y. X. Wang and V. H. Crespi, Nano Lett. **17**(11), 6708–6714 (2017).
[45] A. Azizi, Y. Wang, G. Stone, A. L. Elias, Z. Lin, M. Terrones, V. H. Crespi, and N. Alem, Nano Lett. **17**(5), 2802–2808 (2017).
[46] X.-L. Li, J.-F. Liu, and Y.-D. Li, Appl. Phys. Lett. **81**(25), 4832–4834 (2002).
[47] R. Addou, L. Colombo, and R. M. Wallace, ACS Appl. Mater. Interfaces **7**(22), 11921–11929 (2015).
[48] S. McDonnell, R. Addou, C. Buie, R. M. Wallace, and C. L. Hinkle, ACS Nano **8**(3), 2880–2888 (2014).
[49] R. Addou and R. M. Wallace, ACS Appl. Mater. Interfaces **8**(39), 26400–26406 (2016).
[50] R. Addou and R. M. Wallace, ECS Trans. **79**(1), 11–20 (2017).
[51] W. Müller-Warmuth and R. Schöllhorn, *Progress in Intercalation Research* (Springer Science & Business Media, 2012).
[52] R. Addou, S. McDonnell, D. Barrera, Z. Guo, A. Azcatl, J. Wang, H. Zhu, C. L. Hinkle, M. Quevedo-Lopez, H. N. Alshareef, L. Colombo, J. W. Hsu, and R. M. Wallace, ACS Nano **9**(9), 9124–9133 (2015).
[53] M. S. Dresselhaus, *Intercalation in Layered Materials* (Plenum Press, New York, 1987).
[54] F. Lévy, *Intercalated Layered Materials* (Springer Science & Business Media, 2012).
[55] F. Di Salvo, R. Schwall, T. Geballe, F. Gamble, and J. Osiecki, Phys. Rev. Lett. **27**(6), 310 (1971).
[56] M. J. Wang, I. Al-Dhahir, J. Appiah, and K. J. Koski, Chem. Mater. **29**(4), 1650–1655 (2017).
[57] M. J. Wang and K. J. Koski, ACS Nano **9**(3), 3226–3233 (2015).
[58] K. J. Koski, J. J. Cha, B. W. Reed, C. D. Wessells, D. S. Kong, and Y. Cui, J. Am. Chem. Soc. **134**(18), 7584–7587 (2012).
[59] K. J. Koski, C. D. Wessells, B. W. Reed, J. J. Cha, D. S. Kong, and Y. Cui, J. Am. Chem. Soc. **134**(33), 13773–13779 (2012).
[60] K. P. Chen, F. R. Chung, M. J. Wang, and K. J. Koski, J. Am. Chem. Soc. **137**(16), 5431–5437 (2015).
[61] M. Wang and K. J. Koski, J. Phys.: Condens. Matter **28**(49), 494002 (2016).
[62] B. W. Reed, F. R. Chung, M. J. Wang, T. LaGrange, and K. J. Koski, 2D Mater. **1**(3), 035001 (2014).
[63] A. C. Thenuwara, S. L. Shumlas, N. H. Attanayake, E. B. Cerkez, I. G. McKendry, L. Frazer, E. Borguet, Q. Kang, M. J. Zdilla, J. W. Sun, and D. R. Strongin, Langmuir **31**(46), 12807–12813 (2015).
[64] K. F. Mak, K. He, J. Shan, and T. F. Heinz, Nat. Nanotechnol. **7**(8), 494–498 (2012).
[65] T. Cao, G. Wang, W. Han, H. Ye, C. Zhu, J. Shi, Q. Niu, P. Tan, E. Wang, B. Liu, and J. Feng, Nat. Commun. **3**, 887 (2012).
[66] H. Zeng, J. Dai, W. Yao, D. Xiao, and X. Cui, Nat. Nanotechnol. **7**(8), 490–493 (2012).
[67] G. Sallen, L. Bouet, X. Marie, G. Wang, C. R. Zhu, W. P. Han, Y. Lu, P. H. Tan, T. Amand, B. L. Liu, and B. Urbaszek, Phys. Rev. B **86**(8), 081301 (2012).
[68] A. Srivastava, M. Sidler, A. V. Allain, D. S. Lembke, A. Kis, and A. Imamoglu, Nat. Phys. **11**(2), 141–147 (2015).
[69] G. Aivazian, Z. R. Gong, A. M. Jones, R. L. Chu, J. Yan, D. G. Mandrus, C. W. Zhang, D. Cobden, W. Yao, and X. Xu, Nat. Phys. **11**(2), 148–152 (2015).
[70] D. MacNeill, C. Heikes, K. F. Mak, Z. Anderson, A. Kormanyos, V. Zolyomi, J. Park, and D. C. Ralph, Phys. Rev. Lett. **114**(3), 037401 (2015).
[71] Y. Li, J. Ludwig, T. Low, A. Chernikov, X. Cui, G. Arefe, Y. D. Kim, A. M. van der Zande, A. Rigosi, H. M. Hill, S. H. Kim, J. Hone, Z. Li, D. Smirnov, and T. F. Heinz, Phys. Rev. Lett. **113**(26), 266804 (2014).
[72] E. J. Sie, J. W. McIver, Y. H. Lee, L. Fu, J. Kong, and N. Gedik, Nat. Mater. **14**(3), 290–294 (2015).
[73] J. Kim, X. Hong, C. Jin, S. F. Shi, C. Y. Chang, M. H. Chiu, L. J. Li, and F. Wang, Science **346**(6214), 1205–1208 (2014).
[74] R. Schmidt, A. Arora, G. Plechinger, P. Nagler, A. G. del Aguila, M. V. Ballottin, P. C. M. Christianen, S. M. de Vasconcellos, C. Schuller, T. Korn, and R. Bratschitsch, Phys. Rev. Lett. **117**(7), 077402 (2016).
[75] Z. L. Ye, D. Z. Sun, and T. F. Heinz, Nat. Phys. **13**(1), 26–29 (2017).
[76] A. M. Jones, H. Y. Yu, N. J. Ghimire, S. F. Wu, G. Aivazian, J. S. Ross, B. Zhao, J. Q. Yan, D. G. Mandrus, D. Xiao, W. Yao, and X. D. Xu, Nat. Nanotechnol. **8**(9), 634–638 (2013).
[77] K. F. Mak, K. He, C. Lee, G. H. Lee, J. Hone, T. F. Heinz, and J. Shan, Nat. Mater. **12**(3), 207–211 (2013).
[78] S. Anghel, A. Singh, F. Passmann, H. Iwata, J. N. Moore, G. Yusa, X. Q. Li, and M. Betz, Phys. Rev. B **94**(3), 035303 (2016).
[79] C. H. Lui, A. J. Frenzel, D. V. Pilon, Y. H. Lee, X. Ling, G. M. Akselrod, J. Kong, and N. Gedik, Phys. Rev. Lett. **113**(16), 166801 (2014).
[80] A. Singh, K. Tran, M. Kolarczik, J. Seifert, Y. Wang, K. Hao, D. Pleskot, N. M. Gabor, S. Helmrich, N. Owschimikow, U. Woggon, and X. Li, Phys. Rev. Lett. **117**(25), 257402 (2016).
[81] K. Hao, G. Moody, F. C. Wu, C. K. Dass, L. X. Xu, C. H. Chen, L. Y. Sun, M. Y. Li, L. J. Li, A. H. MacDonald, and X. Q. Li, Nat. Phys. **12**(7), 677–682 (2016).
[82] K. Hao, L. Xu, F. Wu, P. Nagler, K. Tran, X. Ma, C. Schüller, T. Korn, A. H. MacDonald, and G. Moody, 2D Mater. **4**, 025105 (2017).
[83] M. Z. Hasan and C. L. Kane, Rev. Mod. Phys. **82**(4), 3045–3067 (2010).
[84] X. L. Qi and S. C. Zhang, Rev. Mod. Phys. **83**(4), 1057 (2011).
[85] M. Konig, S. Wiedmann, C. Brune, A. Roth, H. Buhmann, L. W. Molenkamp, X. L. Qi, and S. C. Zhang, Science **318**(5851), 766–770 (2007).

[86] L. Du, I. Knez, G. Sullivan, and R. R. Du, Phys. Rev. Lett. **114**(9), 096802 (2015).
[87] E. Y. Ma, M. R. Calvo, J. Wang, B. Lian, M. Muhlbauer, C. Brune, Y. T. Cui, K. Lai, W. Kundhikanjana, Y. Yang, M. Baenninger, M. Konig, C. Ames, H. Buhmann, P. Leubner, L. W. Molenkamp, S. C. Zhang, D. Goldhaber-Gordon, M. A. Kelly, and Z. X. Shen, Nat. Commun. **6**, 7252 (2015).
[88] C. L. Kane and E. J. Mele, Phys. Rev. Lett. **95**(22), 226801 (2005).
[89] S. Murakami, Phys. Rev. Lett. **97**(23), 236805 (2006).
[90] I. K. Drozdov, A. Alexandradinata, S. Jeon, S. Nadj-Perge, H. W. Ji, R. J. Cava, B. A. Bernevig, and A. Yazdani, Nat. Phys. **10**(9), 664–669 (2014).
[91] C. Sabater, D. Gosalbez-Martinez, J. Fernandez-Rossier, J. G. Rodrigo, C. Untiedt, and J. J. Palacios, Phys. Rev. Lett. **110**(17), 176802 (2013).
[92] C. C. Liu, W. Feng, and Y. Yao, Phys. Rev. Lett. **107**(7), 076802 (2011).
[93] Y. Xu, B. Yan, H. J. Zhang, J. Wang, G. Xu, P. Tang, W. Duan, and S. C. Zhang, Phys. Rev. Lett. **111**(13), 136804 (2013).
[94] Z. Y. Fei, T. Palomaki, S. F. Wu, W. J. Zhao, X. H. Cai, B. S. Sun, P. Nguyen, J. Finney, X. D. Xu, and D. H. Cobden, Nat. Phys. **13**(7), 677–682 (2017).
[95] M. J. Mleczko, R. L. Xu, K. Okabe, H. H. Kuo, I. R. Fisher, H. S. Wong, Y. Nishi, and E. Pop, ACS Nano **10**(8), 7507–7514 (2016).
[96] S. J. Tang, C. F. Zhang, D. Wong, Z. Pedramrazi, H. Z. Tsai, C. J. Jia, B. Moritz, M. Claassen, H. Ryu, S. Kahn, J. Jiang, H. Yan, M. Hashimoto, D. H. Lu, R. G. Moore, C. C. Hwang, C. Hwang, Z. Hussain, Y. L. Chen, M. M. Ugeda, Z. Liu, X. M. Xie, T. P. Devereaux, M. F. Crommie, S. K. Mo, and Z. X. Shen, Nat. Phys. **13**(7), 683–687 (2017).
[97] Z.-Y. Jia, Y.-H. Song, X.-B. Li, K. Ran, P. Lu, X.-Y. Zhu, Z.-Q. Shi, J. Sun, J. Wen, and D. Xing, Phys. Rev. B **96**, 041108 (2017).
[98] S. F. Wu, V. Fatemi, Q. D. Gibson, K. Watanabe, T. Taniguchi, R. J. Cava, and P. Jarillo-Herrero, Science **359**(6371), 76–79 (2018).
[99] X. Qian, J. Liu, L. Fu, and J. Li, Science **346**(6215), 1344–1347 (2014).
[100] C. Lee, X. Wei, J. W. Kysar, and J. Hone, Science **321**(5887), 385–388 (2008).
[101] S. Bertolazzi, J. Brivio, and A. Kis, ACS Nano **5**(12), 9703–9709 (2011).
[102] K. He, C. Poole, K. F. Mak, and J. Shan, Nano Lett. **13**(6), 2931–2936 (2013).
[103] G. Plechinger, A. Castellanos-Gomez, M. Buscema, H. S. J. van der Zant, G. A. Steele, A. Kuc, T. Heine, C. Schuller, and T. Korn, 2D Mater. **2**(1), 015006 (2015).
[104] H. J. Conley, B. Wang, J. I. Ziegler, R. F. Haglund, Jr., S. T. Pantelides, and K. I. Bolotin, Nano Lett. **13**(8), 3626–3630 (2013).
[105] Y. Y. Hui, X. Liu, W. Jie, N. Y. Chan, J. Hao, Y. T. Hsu, L. J. Li, W. Guo, and S. P. Lau, ACS Nano **7**(8), 7126–7131 (2013).
[106] J. O. Island, A. Kuc, E. H. Diependaal, R. Bratschitsch, H. S. van der Zant, T. Heine, and A. Castellanos-Gomez, Nanoscale **8**(5), 2589–2593 (2016).
[107] O. B. Aslan, I. M. Datye, M. J. Mleczko, K. S. Cheung, S. Krylyuk, A. Bruma, I. Kalish, A. V. Davydov, E. Pop, and T. F. Heinz, Nano Lett. **18**(4), 2485–2491 (2018).
[108] Y. L. Wang, C. X. Cong, W. H. Yang, J. Z. Shang, N. Peimyoo, Y. Chen, J. Y. Kang, J. P. Wang, W. Huang, and T. Yu, Nano Res. **8**(8), 2562–2572 (2015).
[109] S. B. Desai, G. Seol, J. S. Kang, H. Fang, C. Battaglia, R. Kapadia, J. W. Ager, J. Guo, and A. Javey, Nano Lett. **14**(8), 4592–4597 (2014).
[110] D. Lloyd, X. Liu, J. W. Christopher, L. Cantley, A. Wadehra, B. L. Kim, B. B. Goldberg, A. K. Swan, and J. S. Bunch, Nano Lett. **16**(9), 5836–5841 (2016).
[111] C. Zhu, G. Wang, B. Liu, X. Marie, X. Qiao, X. Zhang, X. Wu, H. Fan, P. Tan, and T. Amand, Phys. Rev. B **88**(12), 121301 (2013).
[112] N. Levy, S. A. Burke, K. L. Meaker, M. Panlasigui, A. Zettl, F. Guinea, A. H. C. Neto, and M. F. Crommie, Science **329**(5991), 544–547 (2010).
[113] T. Low and F. Guinea, Nano Lett. **10**(9), 3551–3554 (2010).
[114] Y. Wu, D. Zhai, C. Pan, B. Cheng, T. Taniguchi, K. Watanabe, N. Sandler, and M. Bockrath, Nano Lett. **18**(1), 64–69 (2018).
[115] S. Manzeli, A. Allain, A. Ghadimi, and A. Kis, Nano Lett. **15**(8), 5330–5335 (2015).
[116] W. Wu, L. Wang, Y. Li, F. Zhang, L. Lin, S. Niu, D. Chenet, X. Zhang, Y. Hao, and T. F. Heinz, Nature **514**(7523), 470 (2014).
[117] A. McCreary, R. Ghosh, M. Amani, J. Wang, K. A. N. Duerloo, A. Sharma, K. Jarvis, E. J. Reed, A. M. Dongare, S. K. Banerjee, M. Terrones, R. R. Namburu, and M. Dubey, ACS Nano **10**(3), 3186–3197 (2016).
[118] H. Li, A. W. Contryman, X. Qian, S. M. Ardakani, Y. Gong, X. Wang, J. M. Weisse, C. H. Lee, J. Zhao, and P. M. Ajayan, Nat. Commun. **6**, 7381 (2015).
[119] H. H. Pérez Garza, E. W. Kievit, G. F. Schneider, and U. Staufer, Nano Lett. **14**(7), 4107–4113 (2014).
[120] J. W. Christopher, M. Vutukuru, D. Lloyd, J. S. Bunch, B. B. Goldberg, D. J. Bishop, and A. K. Swan, preprint arXiv:1803.02787 (2018).
[121] S. B. Desai, S. R. Madhvapathy, M. Amani, D. Kiriya, M. Hettick, M. Tosun, Y. Zhou, M. Dubey, J. W. Ager III, D. Chrzan, and A. Javey, Adv. Mater. **28**(21), 4053–4058 (2016).
[122] W. Haensch, E. J. Nowak, R. H. Dennard, P. M. Solomon, A. Bryant, O. H. Dokumaci, A. Kumar, X. Wang, J. B. Johnson, and M. V. Fischetti, IBM J. Res. Dev. **50**(4-5), 339–361 (2006).
[123] S. Das, A. Prakash, R. Salazar, and J. Appenzeller, ACS Nano **8**(2), 1681–1689 (2014).
[124] S. Das, R. Gulotty, A. V. Sumant, and A. Roelofs, Nano Lett. **14**(5), 2861–2866 (2014).
[125] D. Kim, Y. Lee, J. Cai, I. Lauer, L. Chang, S. J. Koester, D. Sylvester, and D. Blaauw, "Low power circuit design based on heterojunction tunneling transistors (HETTs)," in *ACM/IEEE International Symposium on Low-Power Electronics Design* (Association for Computing Machinery, New York, 2009).

[126] S. Salahuddin and S. Datta, Nano Lett. **8**(2), 405–410 (2008).
[127] S. Das, Sci. Rep. **6**, 34811 (2016).
[128] A. M. Ionescu and H. Riel, Nature **479**(7373), 329–337 (2011).
[129] J. Appenzeller, Y. M. Lin, J. Knoch, and P. Avouris, Phys. Rev. Lett. **93**(19), 196805 (2004).
[130] D. Sarkar, X. J. Xie, W. Liu, W. Cao, J. H. Kang, Y. J. Gong, S. Kraemer, P. M. Ajayan, and K. Banerjee, Nature **526**(7571), 91–95 (2015).
[131] M. W. Si, C. J. Su, C. S. Jiang, N. J. Conrad, H. Zhou, K. D. Maize, G. Qiu, C. T. Wu, A. Shakouri, M. A. Alam, and P. D. Ye, Nat. Nanotechnol. **13**(1), 24 (2018).
[132] F. A. McGuire, Y. C. Lin, K. Price, G. B. Rayner, S. Khandelwal, S. Salahuddin, and A. D. Franklin, Nano Lett. **17**(8), 4801–4806 (2017).
[133] J. Xu, S. Y. Jiang, M. Zhang, H. Zhu, L. Chen, Q. Q. Sun, and D. W. Zhang, Appl. Phys. Lett. **112**(10), 103104 (2018).
[134] D. M. Newns, B. G. Elmegreen, X. H. Liu, and G. J. Martyna, Adv. Mater. **24**(27), 3672–3677 (2012).
[135] V. K. Sangwan, D. Jariwala, I. S. Kim, K. S. Chen, T. J. Marks, L. J. Lauhon, and M. C. Hersam, Nat. Nanotechnol. **10**(5), 403–406 (2015).
[136] A. J. Arnold, A. Razavieh, J. R. Nasr, D. S. Schulman, C. M. Eichfeld, and S. Das, ACS Nano **11**(3), 3110–3118 (2017).
[137] J. Jiang, J. J. Guo, X. Wan, Y. Yang, H. P. Xie, D. M. Niu, J. L. Yang, J. He, Y. L. Gao, and Q. Wan, Small **13**(29), 1700933 (2017).
[138] M. M. S. Aly, M. Gao, G. Hills, C.-S. Lee, G. Pitner, M. M. Shulaker, T. F. Wu, M. Asheghi, J. Bokor, and F. Franchetti, Computer **48**(12), 24–33 (2015).
[139] D. Akinwande, N. Petrone, and J. Hone, Nat. Commun. **5**, 5678 (2014).
[140] E. Pop, Nano Res. **3**(3), 147–169 (2010).
[141] E. Yalon, C. J. McClellan, K. K. H. Smithe, M. Munoz Rojo, R. L. Xu, S. V. Suryavanshi, A. J. Gabourie, C. M. Neumann, F. Xiong, A. B. Farimani, and E. Pop, Nano Lett. **17**(6), 3429–3433 (2017).
[142] S. V. Suryavanshi and E. Pop, J. Appl. Phys. **120**(22), 224503 (2016).
[143] S. Islam, Z. Y. Li, V. E. Dorgan, M. H. Bae, and E. Pop, IEEE Electron Device Lett. **34**(2), 166–168 (2013).
[144] C. D. English, G. Shine, V. E. Dorgan, K. C. Saraswat, and E. Pop, Nano Lett. **16**(6), 3824–3830 (2016).
[145] K. L. Grosse, M. H. Bae, F. F. Lian, E. Pop, and W. P. King, Nat. Nanotechnol. **6**(5), 287–290 (2011).
[146] C. C. Chen, Z. Li, L. Shi, and S. B. Cronin, Appl. Phys. Lett. **104**(8), 081908 (2014).
[147] C. D. English, K. K. Smithe, R. L. Xu, and E. Pop, in *IEEE International Electron Device Meeting (IEDM)* (IEEE, 2016).
[148] C. J. McClellan, E. Yalon, K. K. H. Smithe, S. V. Suryavanshi, and E. Pop, in *IEEE Device Research Conference (DRC)* (IEEE, 2017).
[149] K. K. Smithe, C. D. English, S. V. Suryavanshi, and E. Pop, 2D Mater. **4**(1), 011009 (2016).
[150] S. Hao, B. C. Yang, and Y. L. Gao, J. Appl. Phys. **120**(12), 124310 (2016).
[151] Y. L. Huang, Y. F. Chen, W. J. Zhang, S. Y. Quek, C. H. Chen, L. J. Li, W. T. Hsu, W. H. Chang, Y. J. Zheng, W. Chen, and A. T. S. Wee, Nat. Commun. **6**, 6298 (2015).
[152] E. Yalon, O. B. Aslan, K. K. H. Smithe, C. J. McClellan, S. V. Suryavanshi, F. Xiong, A. Sood, C. M. Neumann, X. Q. Xu, K. E. Goodson, T. F. Heinz, and E. Pop, ACS Appl. Mater. Interfaces **9**(49), 43013–43020 (2017).
[153] C. Monachon, L. Weber, and C. Dames, Annu. Rev. Mater. Res. **46**, 433–463 (2016).
[154] See http://www.itrs2.net for information about the International Technology Roadmap for Semiconductors.
[155] R. Mehta, S. Chugh, and Z. Chen, Nano Lett. **15**(3), 2024–2030 (2015).
[156] G. S. Haase, E. T. Ogawa, and J. W. McPherson, J. Appl. Phys. **98**(3), 034503 (2005).
[157] L. Zhao, Z. Tokei, K. Croes, C. J. Wilson, M. Baklanov, G. P. Beyer, and C. Claeys, Appl. Phys. Lett. **98**(3), 032107 (2011).
[158] N. Suzumura, S. Yamamoto, D. Kodama, K. Makabe, J. Komori, E. Murakami, S. Maegawa, and K. Kubota, in *IEEE International Reliability Physics Symposium Proceedings (IRPS)* (IEEE, 2006).
[159] F. Chen, O. Bravo, K. Chanda, P. McLaughlin, T. Sullivan, J. Gill, J. Lloyd, R. Kontra, and J. Aitken, in *IEEE International Reliability Physics Symposium Proceedings (IRPS)* (IEEE, 2006).
[160] K. Croes, P. Roussel, Y. Barbarin, C. Wu, Y. Li, J. Bömmels, and Z. Tőkei, in *IEEE International Reliability Physics Symposium (IRPS)* (IEEE, 2013).
[161] C.-L. Lo, S. Zhang, T. Shen, J. Appenzeller, and Z. Chen, in *IEEE Device Research Conference (DRC)* (IEEE, 2017).
[162] C.-L. Lo, K. K. Smithe, R. Mehta, S. Chugh, E. Pop, and Z. Chen, in *IEEE International Reliability Physics Symposium (IRPS)* (IEEE, 2017).
[163] C. L. Lo, M. Catalano, K. K. H. Smithe, L. H. Wang, S. J. Zhang, E. Pop, M. J. Kim, and Z. H. Chen, npj 2D Mater. Appl. **1**, 42 (2017).
[164] Y. Saito, T. Nojima, and Y. Iwasa, Nat. Rev. Mater. **2**(1), 16094 (2017).
[165] N. Samarth, Nature **546**(7657), 216–218 (2017).